SAM SAFER

WP4 Fuel Salt Confinement

Final project meeting

28 November 2023 - 30 November 2023

Task 4.1 *Improvement of melting/solidification modelling capabilities*

1. An energy-conservative DG-FEM approach for solid-liquid phase change
   - DG-FEM numerical method with arbitrarily high order of accuracy, possibility for upwinding, local conservation of variables, high parallelization efficiency and high geometric flexibility.
   - Based on conservative form of the energy equation, energy-conservation guaranteed through convergence criterion.
2. A finite-volume parallel adaptive mesh refinement method for solid-liquid phase change
   - Solid-liquid interface and flow recirculation zones resolved with a locally high resolution through adaptive mesh refinement.
   - Three different refinement criteria were constructed, based on the maximum difference in the liquid fraction over the cell faces, and the estimated numerical discretization error in the flow and temperature fields.
   - High parallelization efficiency was maintained through a dynamic load balancing step following each change to the mesh.

The linearized enthalpy approach

- Non-linear enthalpy-temperature coupling solved through first order Taylor linearization of the volumetric enthalpy and a set of Newton iterations.
- Darcy source term used to account for no-slip condition at solid-liquid interface in momentum equation.
- Use of a mushy zone is optional.
- Global energy-conservation check is performed as part of the energy convergence criterion.

$$\frac{\partial H}{\partial t} + v_i \frac{\partial H}{\partial x_i} = \frac{\partial}{\partial x_i}\left(\lambda \frac{\partial T}{\partial x_i}\right)$$

$$(H)^{k+1} \approx (H)^k + \left.\frac{\partial H}{\partial T}\right|^k \left(T^{k+1,*} - T^k\right)$$

$$T = \begin{cases} \dfrac{H}{\rho_s c_{p,s}}, & H < \rho_s c_{p,s} T_m \\ T_m, & \rho_s c_{p,s} T_m \le H \le \rho_s c_{p,s} T_m + \rho_l \Delta H_f \\ T_m + \dfrac{H - (\rho_s c_{p,s} T_m + \rho_{l,s} \Delta H_f)}{\rho_l c_{p,l}}, & H > \rho_s c_{p,s} T_m + \rho_l \Delta H_f \end{cases}$$

$$\frac{\partial(\rho_l v_i)}{\partial t} + v_j \frac{\partial(\rho_l v_i)}{\partial x_j} = \frac{\partial}{\partial x_j}\left[\mu\left(\frac{\partial v_i}{\partial x_j} + \frac{\partial v_j}{\partial x_i}\right)\right] - \frac{\partial p}{\partial x_i} + \rho_l g_i \beta (T - T_m) + S_u$$

$$S_u = -C \frac{(1-\alpha)^2}{\alpha^3 + b} u$$

SAM SAFER TU Delft

DG-FEM melting and solidification modelling framework

- Mixed order formulation: $P_p = P_u - 1$.
- Convection terms discretized with Lax-Friedrichs numerical flux, diffusion term discretized with symmetric interior penalty method (SIP).
- Time derivatives discretized with BDF2.

$$Find \quad m_h \in \mathcal{V}_{h,m}^d \quad and \quad p_h \in \mathcal{V}_{h,p,H,T} \quad and \quad H_h \in \mathcal{V}_{h,p,H,T} \quad and \quad T_h \in \mathcal{V}_{h,p,H,T}$$
$$such \quad that \quad \forall v_h \in \mathcal{V}_{h,m}^d \quad and \quad \forall q_h, \forall w_h \in \mathcal{V}_{h,p,H,T},$$

$$\sum_{\mathcal{T} \in \mathcal{T}_h} \int_{\mathcal{T}} \boldsymbol{v}_h \cdot \frac{\partial \boldsymbol{m}_h}{\partial t} + a^{conv}(\boldsymbol{u}_h, \boldsymbol{m}_h, \boldsymbol{v}_h) + a^{diff}(\boldsymbol{m}_h, \boldsymbol{v}_h) + a^{div}(\boldsymbol{v}_h, p_h)$$
$$+ a^{source}(\boldsymbol{m}_h, \boldsymbol{v}_h) = l^{conv}(\boldsymbol{u}_h, m_k^D \mathbf{v}_h) + l^{diff}(\boldsymbol{v}_h) + l^{source}(\boldsymbol{v}_h, T_h)$$
$$a^{div}(\boldsymbol{m}_h, q_h) = l^{div}(q_h)$$
$$\sum_{\mathcal{T} \in \mathcal{T}_h} \int_{\mathcal{T}} w_h \frac{\partial H_h}{\partial t} + a^{conv}(\boldsymbol{m}_h, T_h, w_h) + a^{diff}(T_h, w_h)$$
$$= l^{conv}(\boldsymbol{u}_h, w_h) + l^{diff}(w_h)$$
$$T_h = T(H_h).$$

Case 1: 1D Stefan problem

- Numerical results compared with analytical solution.
- O(h) convergence obtained for both linear and quadratic elements.

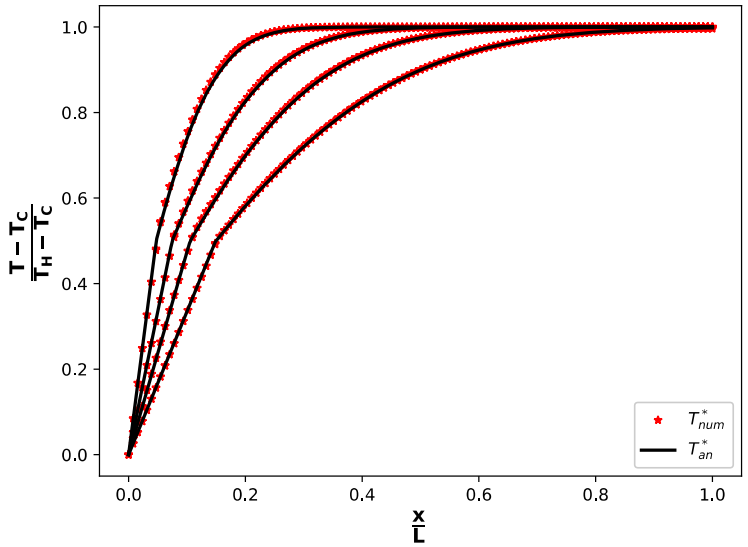

Temperature field at 100, 250, 500 and 1000 s.

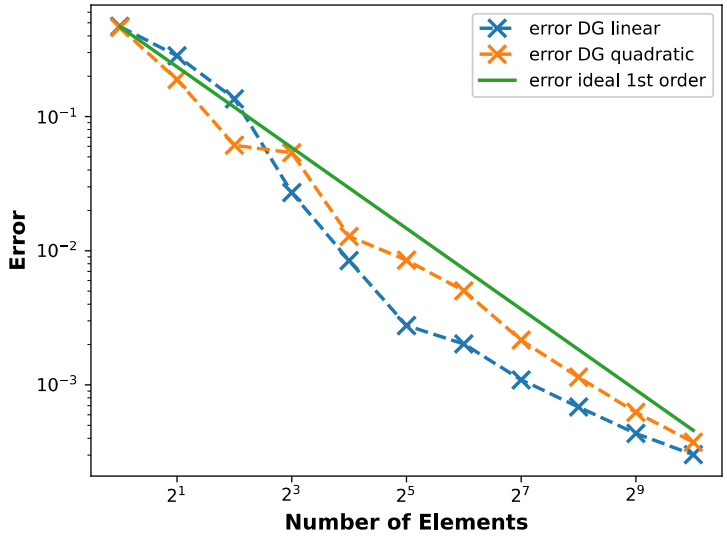

Relative L^2 norms for the error in the temperature field at 250 s, plotted for an increasing number of elements.

SAM SAFER

Case 2: Melting of octadecane in a square cavity

- Recent experimental data available.
- Good agreement was obtained with experimental and numerical reference solution.
- Again, suboptimal O(h) convergence was observed.
- Increasing the order of the elements made little difference.

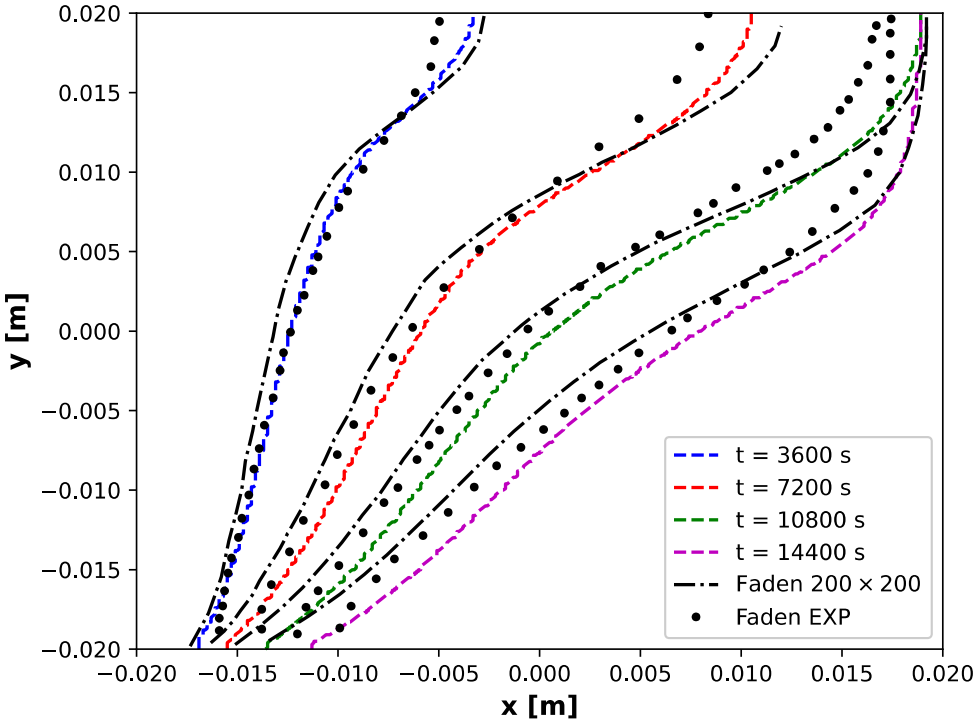

Interface position at respectively 3600 s, 7200 s, 10800 s, 14400 s. The mesh consists of 200×200 $P = \{2,1,1,1\}$ *elements. BDF2 time-stepping with a time step of* $\Delta t = 0.25\ s$ *was used.*

SAM SAFER

Test case: melting of gallium in a rectangular enclosure

- Classic numerical benchmark for melting simulations.
- Strict mesh requirements due to multicellular flow patterns.
- This problem benefited from the use of higher order elements.

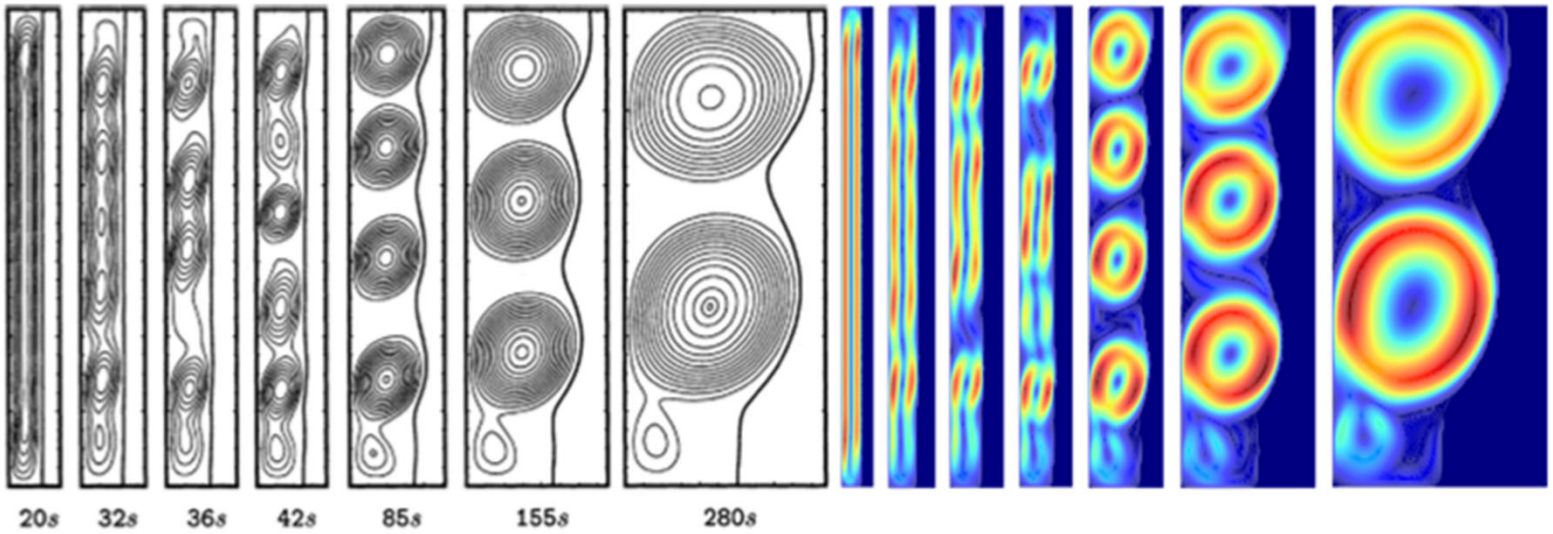

Absolute velocity contours at 20 s, 32 s, 36 s, 42 s, 85 s. The mesh consists of 280×200 $P = \{3,2,2,2\}$ *elements. BDF2 time-stepping with a time step of* $\Delta t = 0.025\ s$ *was used. The right side shows the results from the current numerical campaign, the left side depicts the reference solution.*

A finite volume parallel adaptive mesh refinement method for solid-liquid phase change

- Dynamic mesh library of OpenFOAM v9 (enhanced version):
  - Quadtree / octtree refinement and coarsening of arbitrary 2D and 3D element shapes.
  - Pressure correction ensure a divergence free mass flux field following each refinement/coarsening step.
  - Dynamic load balancing procedure to maintain a high parallelization efficiency.
- Multiple refinement criteria:
  1. Refinement of the interface based on the maximum difference in the liquid fraction over the cell faces.
  2. Refinement based on the estimated relative numerical discretization error (using the cell residual method) in the flow and temperature fields.

Demonstration: melting of gallium in a rectangular enclosure.

- Adaptive mesh using a 70×50 background mesh with 4 levels of refinement.
- Excellent agreement obtained between the uniform reference solution and the adaptive mesh using significantly less degrees of freedom.

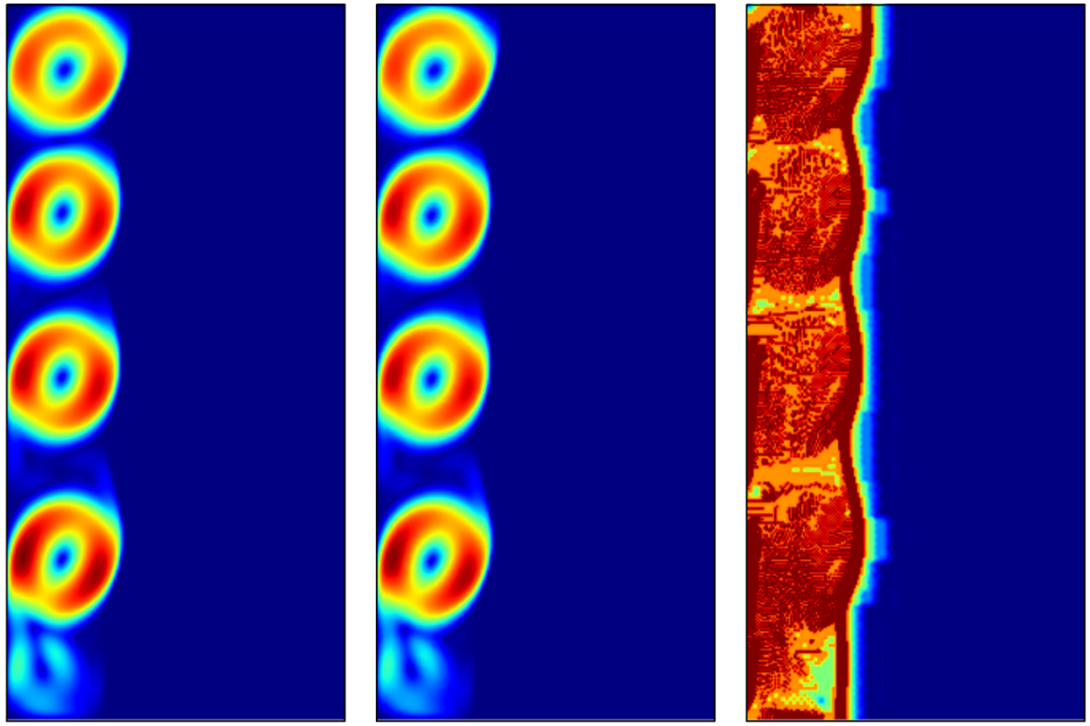

From left to right: absolute velocity contour at 85 s on a 1120×800 uniform mesh, absolute velocity contour on the adaptive mesh, cell level of the adaptive mesh showing the pattern of refinement. Adaptive mesh has 65,141 elements in total.

SAM SAFER

Conclusions Task 4.1

- Despite the arbitrarily high order of accuracy, the current DG-FEM melting and solidification modelling approach yielded an overal O(h) mesh convergence rate.
- Mainly solid-liquid phase change problems with strong gradients in the flowfield can benefit from the proposed higher order DG-FEM method.
- Promising results were obtained using the finite volume parallel adaptive mesh refinement solver for solid-liquid phase change problems, obtaining accurate solutions at significantly reduced computational cost.

Dissemination Task 4.1

Deliverables

- D4.1 Advanced phase change model representation and implementation (**completed)**

Conferences

- B.J. Kaaks, J.W.A. Reus, M. Rohde, J.L. Kloosterman and D. Lathouwers. Numerical study of phase change phenomena: a conservative linearized enthalpy approach. In: *Proc. 19th International Topical Meeting on Nuclear Reactor Thermal Hydraulics (NURETH 19)*. Brussels, Belgium(2022).

Journal papers

- B.J. Kaaks, M. Rohde, J.L. Kloosterman and D. Lathouwers. An energy-conservative DGFEM approach for solid–liquid phase change, *Numerical Heat Transfer, Part B: Fundamentals* 84 (2023). doi:10.1080/10407790.2023.2211231.
- B.J.Kaaks, J.L. Kloosterman, M. Rohde, D. Lathouwers. A finite volume parallel adaptive mesh refinement method for solid-liquid phase change, *Numerical Heat Transfer, Part B: Fundamentals* (2023). *Under review.*

Relevant numerical data, FVM & DG-FEM numerical solvers for 1D Stefan problem, and AMR OpenFOAM phase change solvers shared in SAMOSAFER Zenodo community.

Modelling approach for melting/solidification

. Development of an OpenFOAM solver for modelling melting and solidification to be included in the current solver

. Fixed grid approach

. Velocity Transition Modelling for momentum equation (Darcy Source Term)

$$\frac{\partial(\rho\vec{u})}{\partial t} + \nabla\cdot(\rho\vec{u}\vec{u}) = -\nabla P + \nabla\cdot\left(\mu_l\frac{\rho}{\rho_l}\nabla\vec{u}\right) + \rho\vec{g} - \frac{\mu_l}{K}\frac{\rho}{\rho_l}(\vec{u}-\vec{u}_s)$$

. T-based latent heat modelling

$$\frac{\partial(\rho h)}{\partial t} + \nabla\cdot(\rho_l T\vec{u}) = \nabla\cdot(k\nabla T)$$

$$h = h(f,T),\ f = (h,T)$$

. Conduction and convection

Modelling approach for melting/solidification

Apparent heat capacity method

$$\frac{\partial(\rho h)}{\partial t} \propto H_p - H_p^{old} = \left[\frac{\mathrm{d}H}{\mathrm{d}T}\right]_p \left(T_p - T_p^{old}\right)$$

. $\left[\frac{\mathrm{d}H}{\mathrm{d}T}\right]_p$ depends on the choosen closure relationship between T and H (or T and g)

. Fast (non-iterative)

. Prone to inaccurate results (skip of latent heat peak)

. More sensitive to arbitrary modelling parameters

Source Term

$$\frac{\partial(\rho h)}{\partial t} \propto \left[\rho_s C_{ps} + g^m \Delta(\rho C_P)\right] \frac{\partial T^{m+1}}{\partial t} + \\ + \Delta\left(\rho C_p\right) \frac{\partial g^m}{\partial t} \cdot T^{m+1} + \rho_l \lambda \frac{\partial g^m}{\partial t}$$

. Express H as a function of g and T only, evaluate g at the previous iteration (g^m)

. Iterative (slow)

. Less sensitive to modelling parameters

. Robust method

Hybrid method:

Apparent heat capacity as default + check on the latent heat peak skip (from T < T_s to T > T_l) → move to source term

SAM SAFER

Verification of conduction solver with analytical solution

. 1D case: finite slab, $0 \leq x \leq L$
. Material properties: $LiF - ThF_4$
. Melting problem: initially solid, melts from left to right
. Check against analytical solution of the Stefan Problem

Property *	$LiF - ThF_4$	
	Solid	Liquid
Thermal conductivity (W m^{-1} K^{-1})	1.5	1.5
Density (kg m^{-3})	4502	4390
Specific heat capacity (J kg^{-1} K^{-1})	815	1000
Latent heat (J kg^{-1})	$1.59 \cdot 10^5$	
Melting temperature (K)	841	

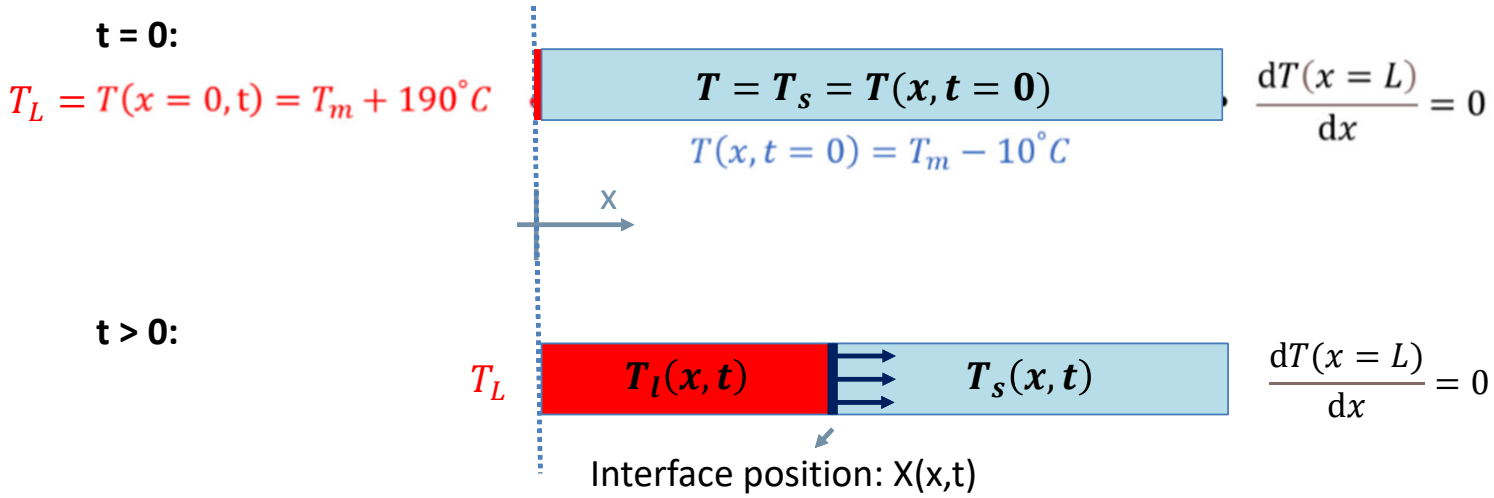

* M. Tiberga, et al., 2019. "Preliminary investigation on the melting behavior of a freeze-valve for the Molten Salt Fast Reactor," Annals of Nuclear Energy, 132, 544-554

Verification of conduction solver with analytical solution

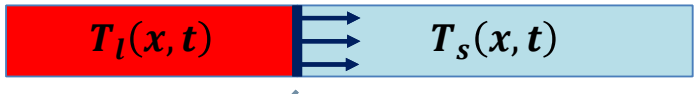

Interface position: X(x,t)

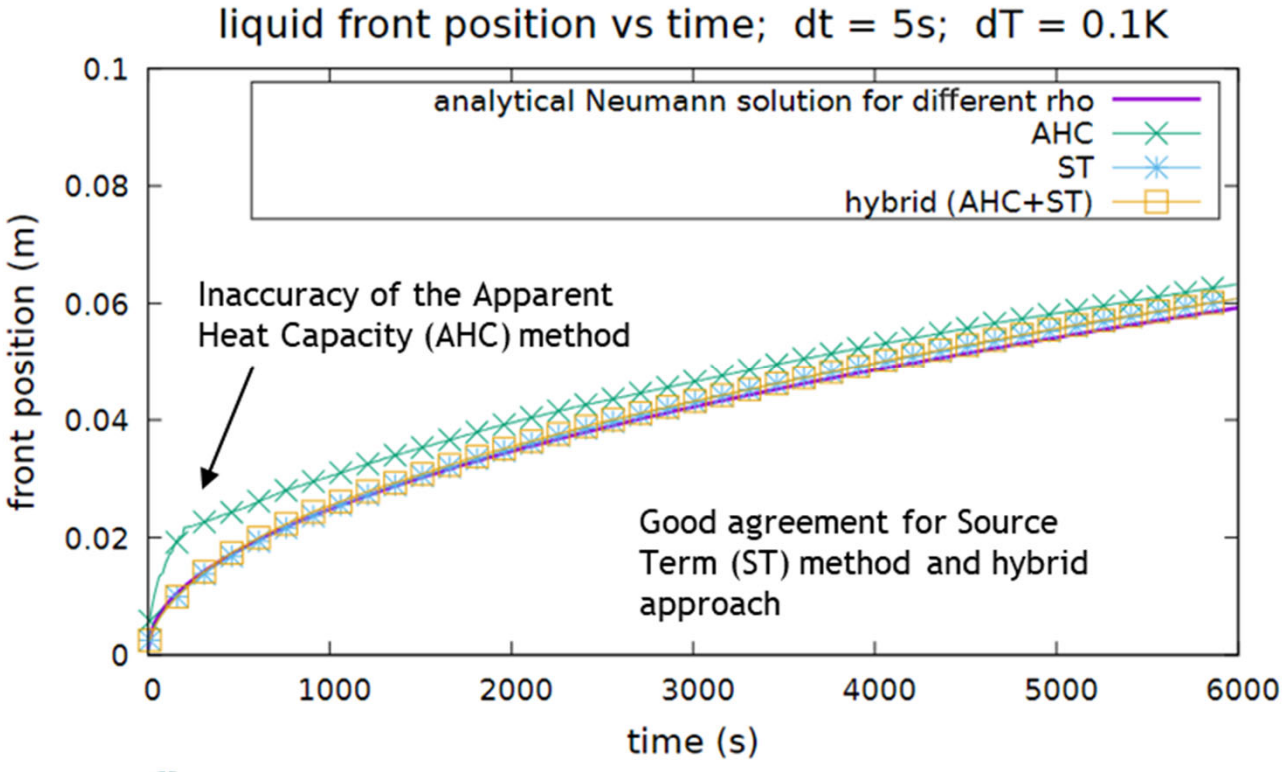

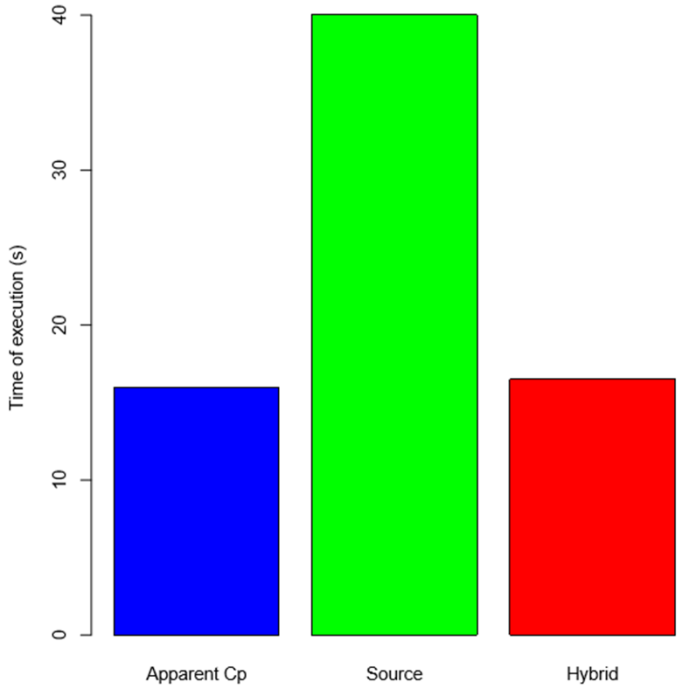

Verification of conduction&convection solver with numerical solution

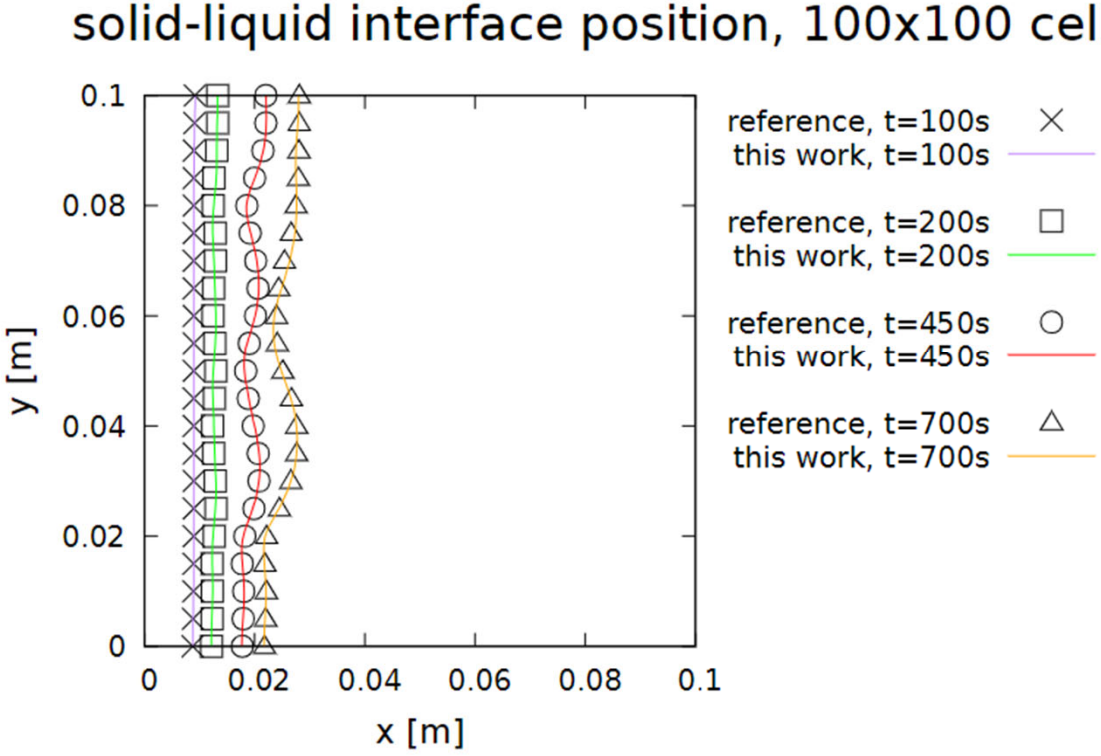

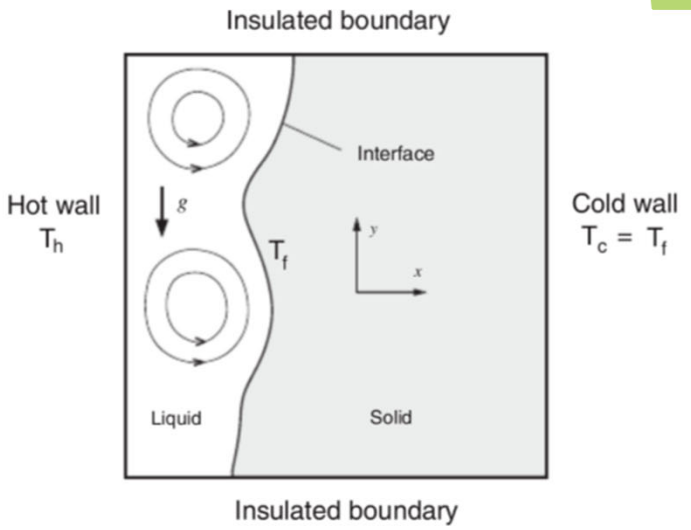

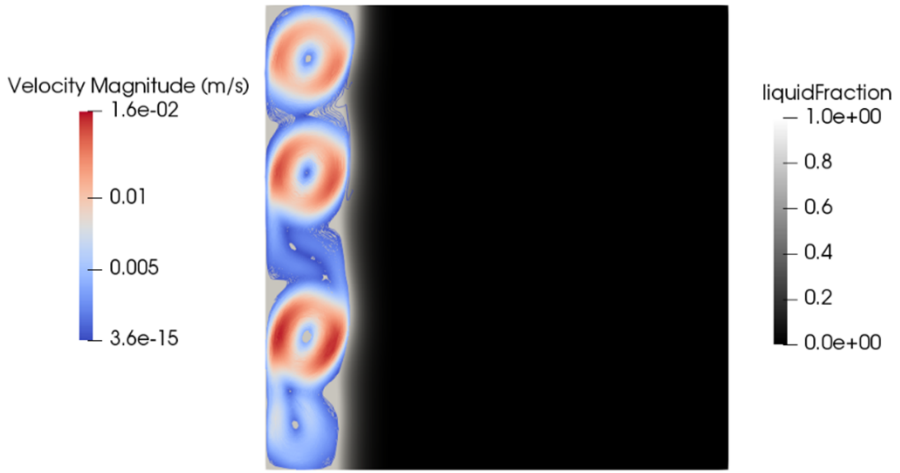

SAM SAFER

Freeze plug-like simulation

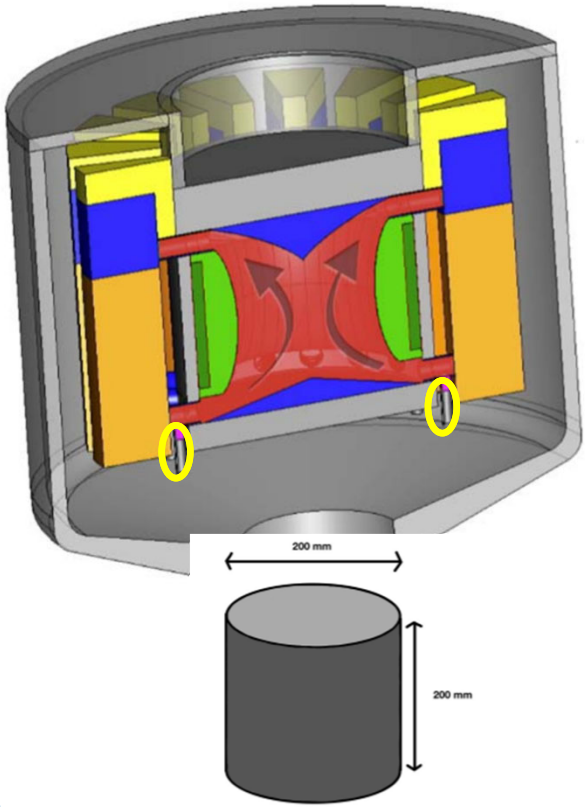

Nominal conditions

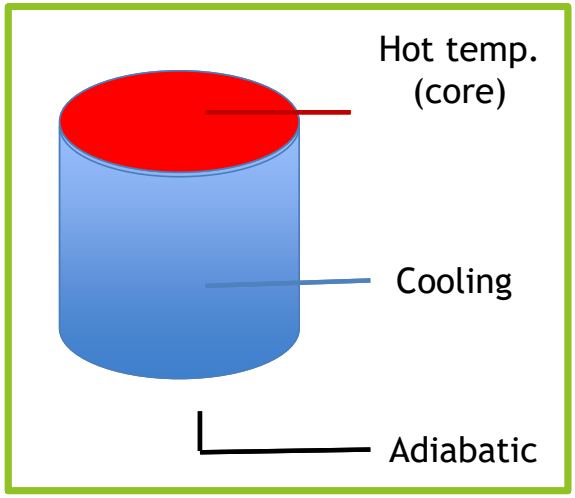

Accidental conditions

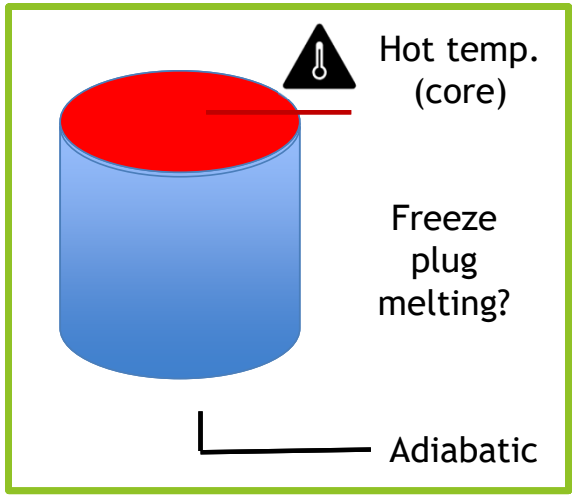

Results strongly depend on the BC on the velocity

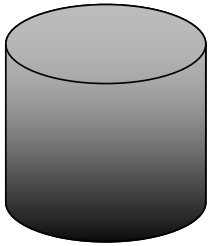

Pure Heat
Conduction

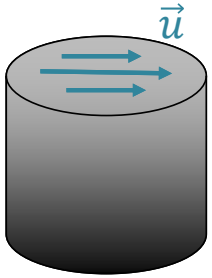

Convection

SAM SAFER

Freeze plug-like simulation

Results strongly depend on the BC on the velocity – Accidental condition

. Melting time in adiabatic conditions is very long (over 10,000 s for conduction, around 1,000 s for convection)

. In nominal conditions, modest subcooling allows closure of valve

. Effects of convection, when present, are dominant on the melting time

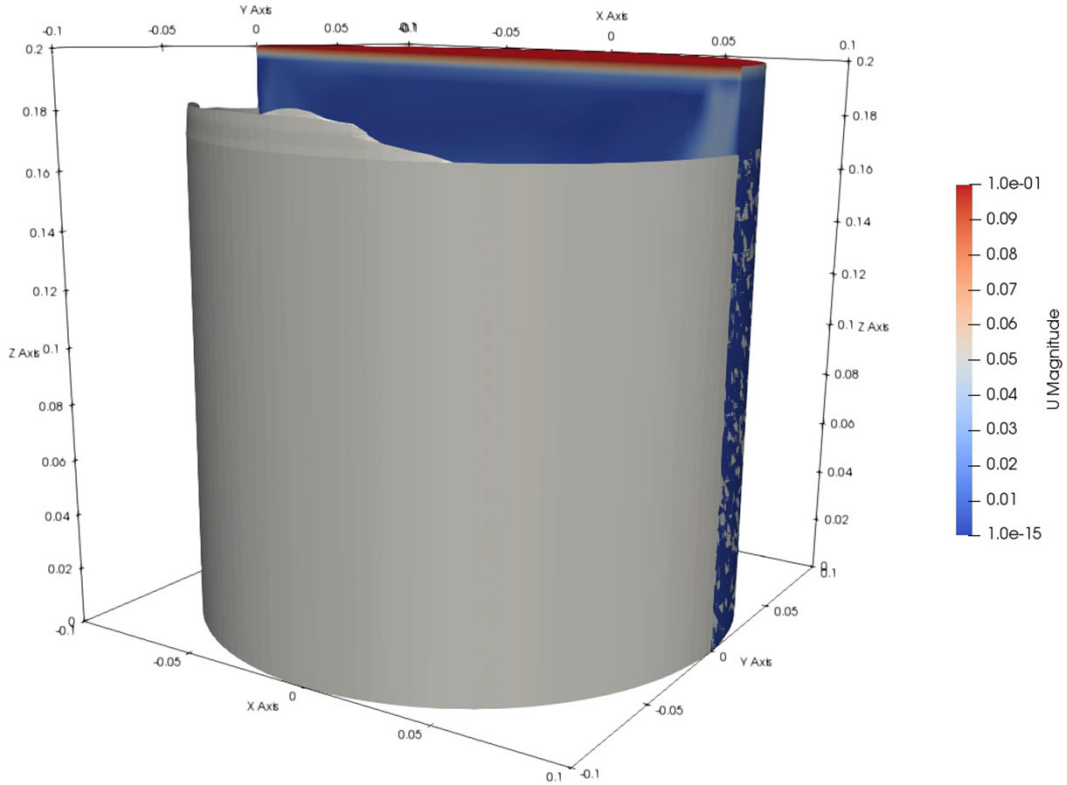

SAM SAFER

Task 4.2 *Experimental Validation of Melting/Solidification Modelling Capabilities*

1. An experimental setup (ESPRESSO) was designed and built for transient ice-growth experiments in forced internal flow.
2. Particle image velocimetry (PIV) measurements were performed of transient ice growth in a laminar channel flow, for both the inlet and the center of the channel where the heat transfer becomes near one-dimensional.
3. A good agreement was obtained between the generated experimental data and numerical simulations, performed with the developed DG-FEM based solid-liquid phase change solver.

Design of experimental facility (ESPRESSO)

- Rectangular duct ($\mathrm{h} \times b \times l = 5 \times 5 \times 145\ cm$) made of PMMA to guarantee optical acess.
- Water flow controlled by pump with an electronic frequency drive, maximum flow rate is 1.4 L/s.
- Cold plate (offset fin design) capable of reaching -20 ° C.
- Precooling of inlet through brazed plate liquid heat exchanger to a minimum temperature of 0 ° C.
- Combination of converging nozzle and settling chamber with honeycomb grid and turbulence reduction screens for imposing uniform inlet condition.
- Sensors are included for recording the cold-plate, inlet and outlet temperatures, as well as the flow-rate.

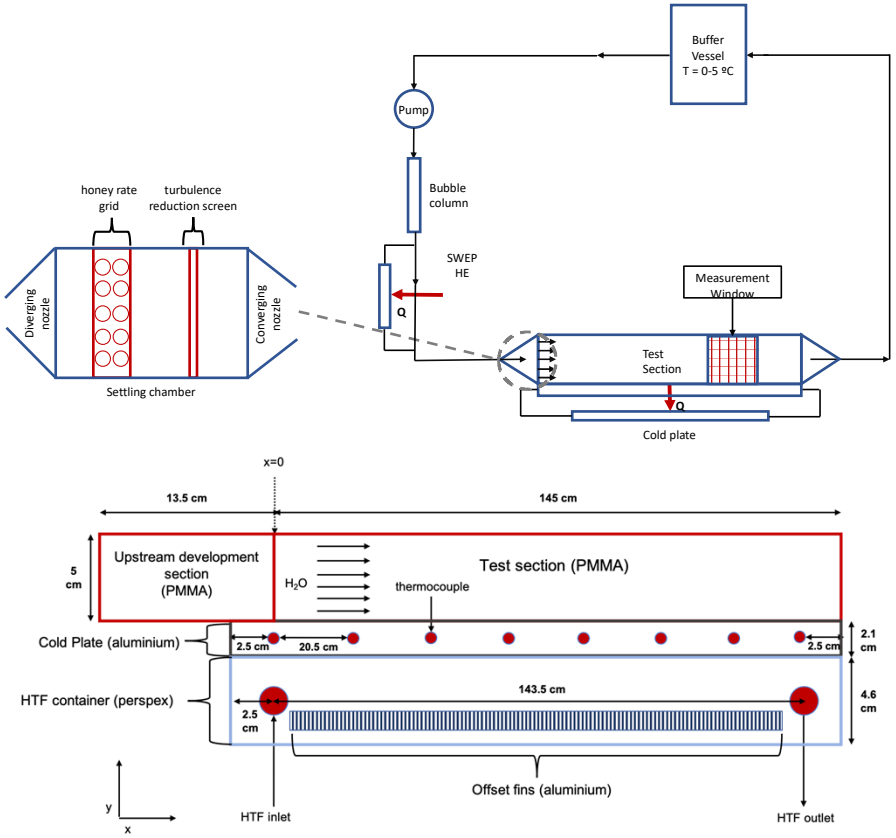

Design schematics of the ESPRESSO facility: entire loop (top) and zoom in of the test section and the heat sink (bottom).

SAM SAFER TU Delft

Finalized experimental facility (ESPRESSO)

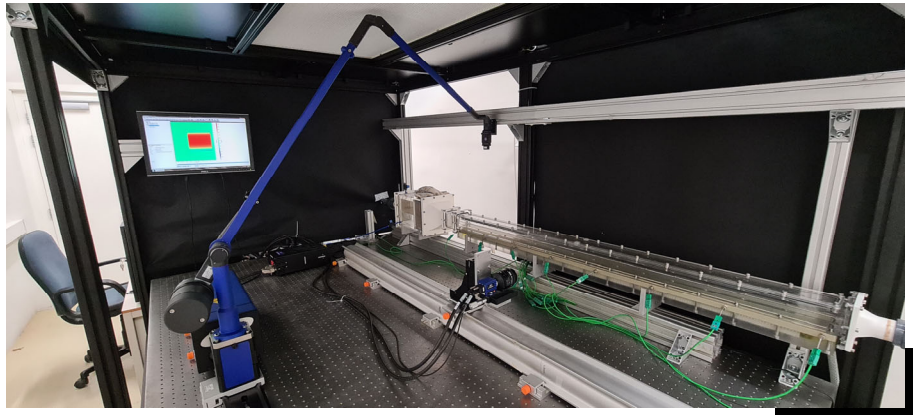

- Planar PIV.
- 5W shuttered continuous laser (diode pumped, 532 nm).
- High speed CMOS camera (LaVision MX4M).
- Borosilicate glass particle seeding (1.1 gcm^{-3}, 9-13 μm, Stk = 1.5E-6 for Re = 500).

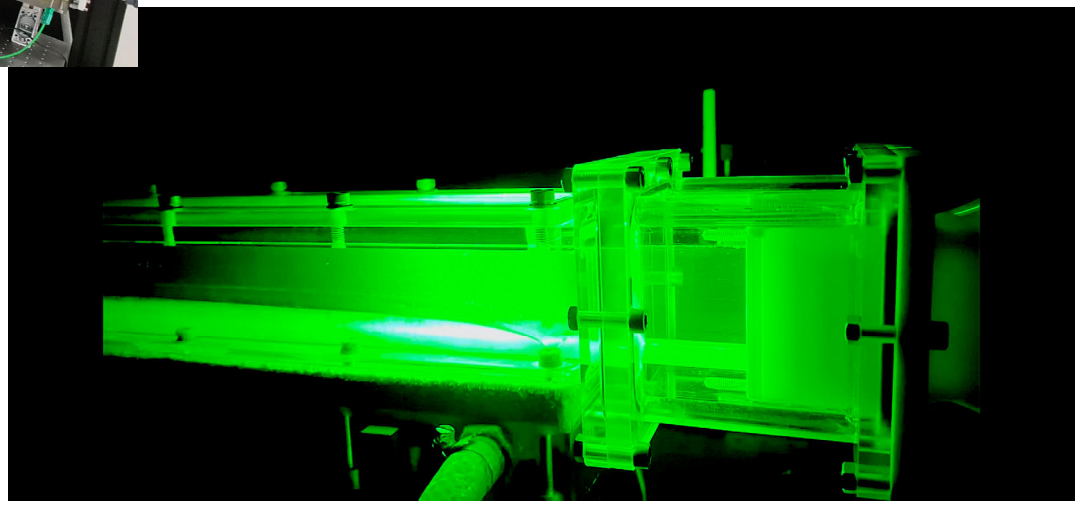

SAM SAFER TU Delft

Visualization of Ice-Layer

- Growth of ice-layer from cold-plate succesful.
- Ice-layer well visualized with laser-sheet illumination and CMOS camera.
- Experimental challenges:
  1) Reflections from aluminum cold plate, perspex walls, and ice-layer.
  2) Blind spots laser and camera (due to screws, o'ring grooves etc).
  3) Uneven illumination from laser sheet.
  4) Condens formation on perspex walls due to cold temperatures.
  5) Determination of exact onset of ice-formation.

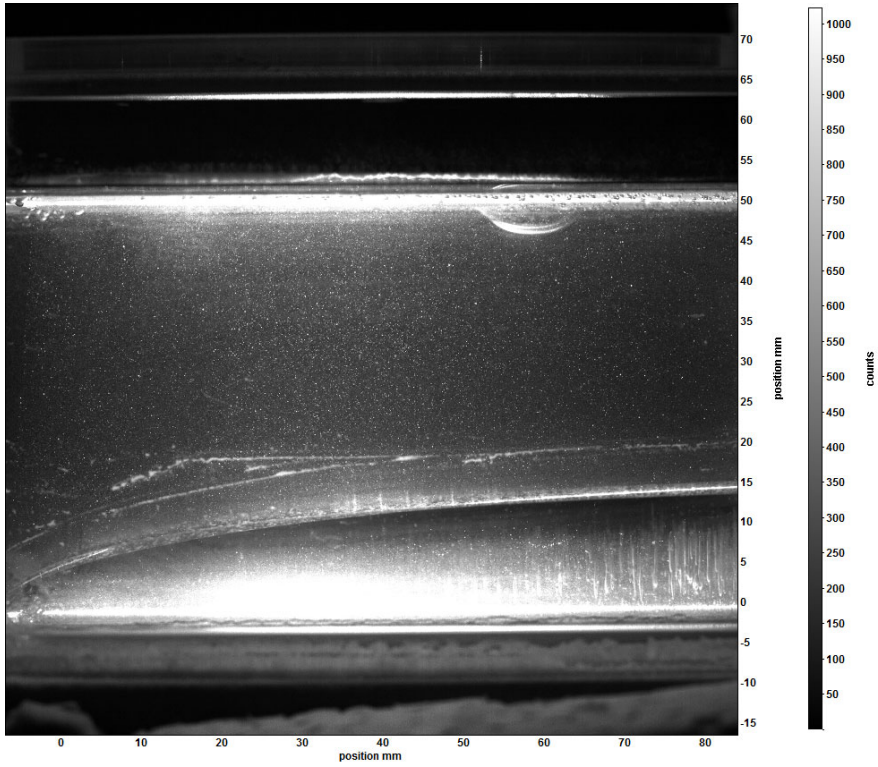

Ice-layer after 90 min for Re ≈ 474, T_{in} ≈ 5 °C, T_{set} ≈ -10 °C.

SAM SAFER TU Delft

Flowfield

- Image pre-processing: non-linear sliding average substraction (filter size = 5 pixel) followed by a min-max filter and an intensity normalization filter.
- Vector calculation: Multi-pass: 3 x (64 x 64) with 75% overlap, 1 x (32 x 32) with 50% overlap
- Postproccessing: removal of outliers through median filter and specification of out of bounds velocity values, followed by a statistical averaging and a 3×3 Gaussian smoothing filter.
- Acceleration of bulk flow as ice-layer grows.
- Theory predicts: heat transfer from fluid to solid-liquid interface increases, heat transfer from cold plate to ice-layer decreases as the ice-layer thickens. Steady state solution for certain parameter combinations.

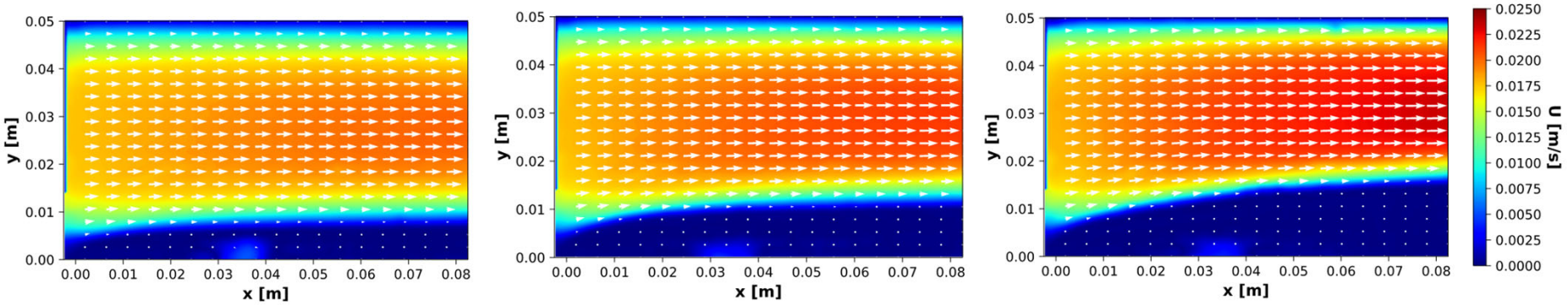

Flowfield after respectively 10, 30 and 90 min for Re ≈ 474, T_{in} ≈ 5 °C, T_{set} = -10 °C.

SAM SAFER TU Delft

Determination of Experimental Boundary Condition

- Cold plate temperatures recorded by 8 equally spaced thermo couples
- Onset of ice-formation marked by a sudden sharp increase of the cold-plate temperature, used to determine the zero-time instant in our experiments.
- Sequence of the thermocouples' response showed that ice nucleation first occurs at the inlet of the channel, from which the ice subsequently spreads over the entire cold plate surface.
- Fit used to describe temperature evaluation of the cold-plate in time, used as input for numerical simulations.

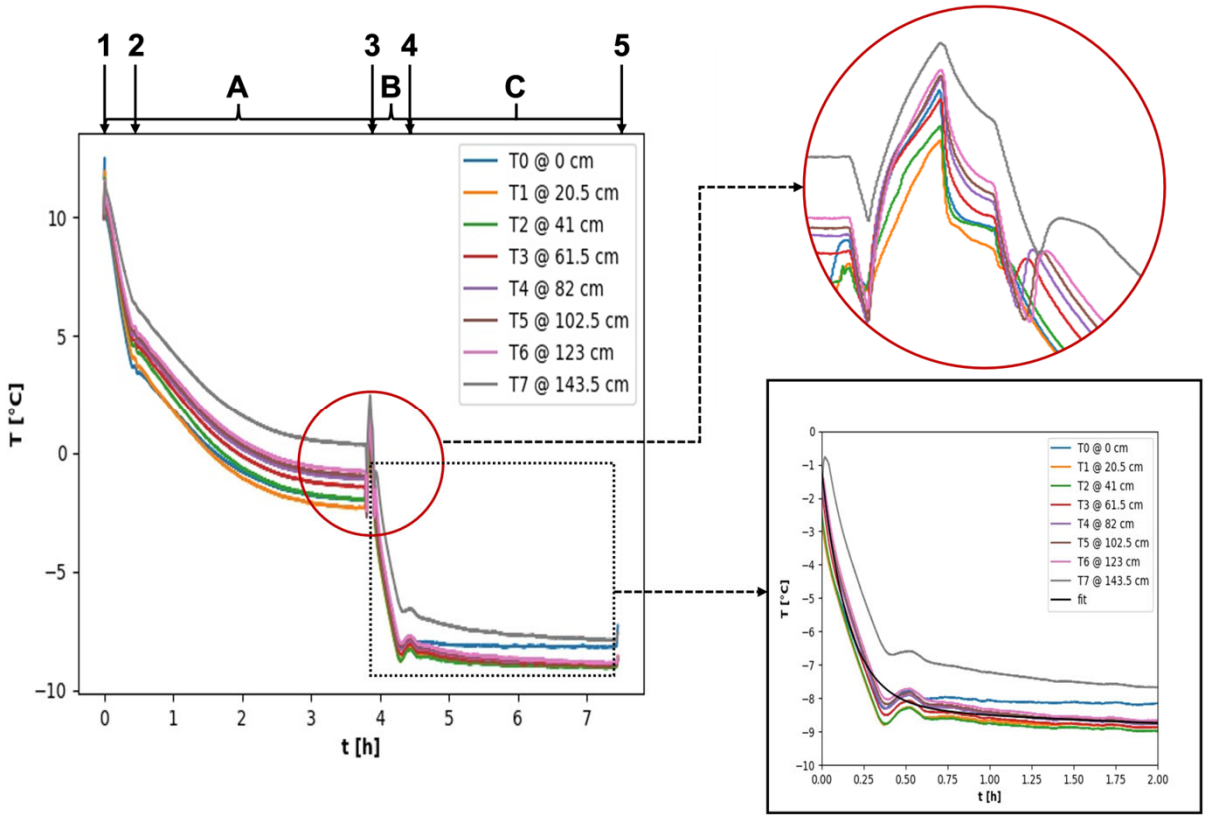

Temperature response of the cold plate, and resulting fit function.

SAM SAFER

Comparison of Experimental Results with Numerical Simulations

- 2D numerical domain.
- Linearized enthalpy approach with DG-FEM.
- Constant thermophysical properties for each phase (except for the thermal expansion coefficient) and use of Boussinesq approximation.
- Extension of inlet and outlet to avoid issues with inlet and outlet boundary conditions due to growth of the ice-layer

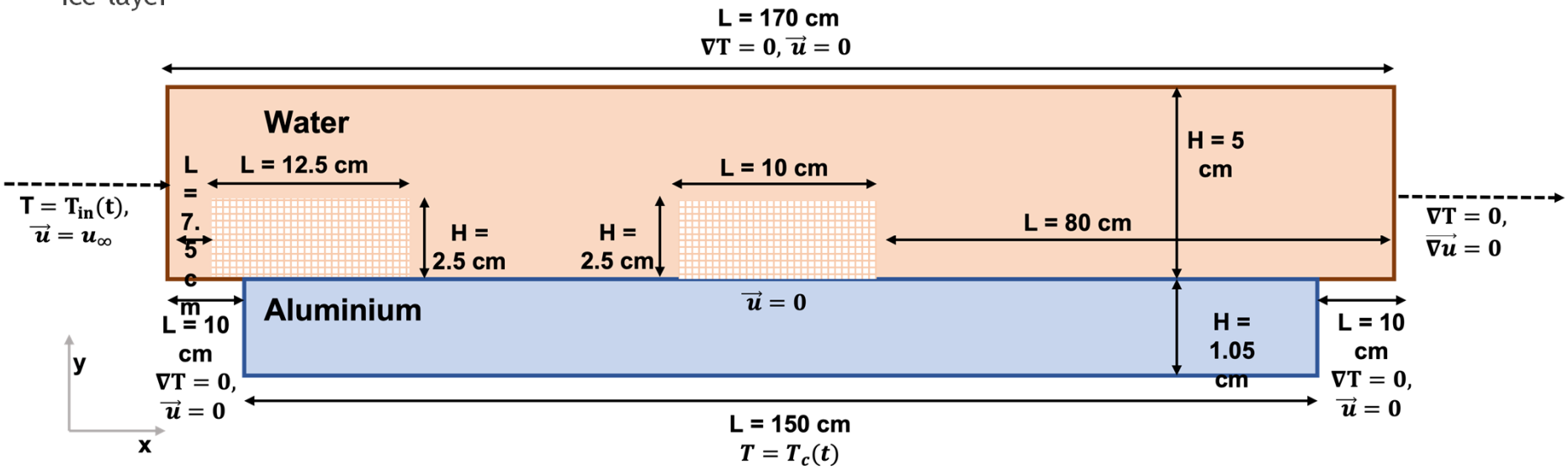

Computational domain.

Comparison of Experimental Results with Numerical Simulations (inlet)

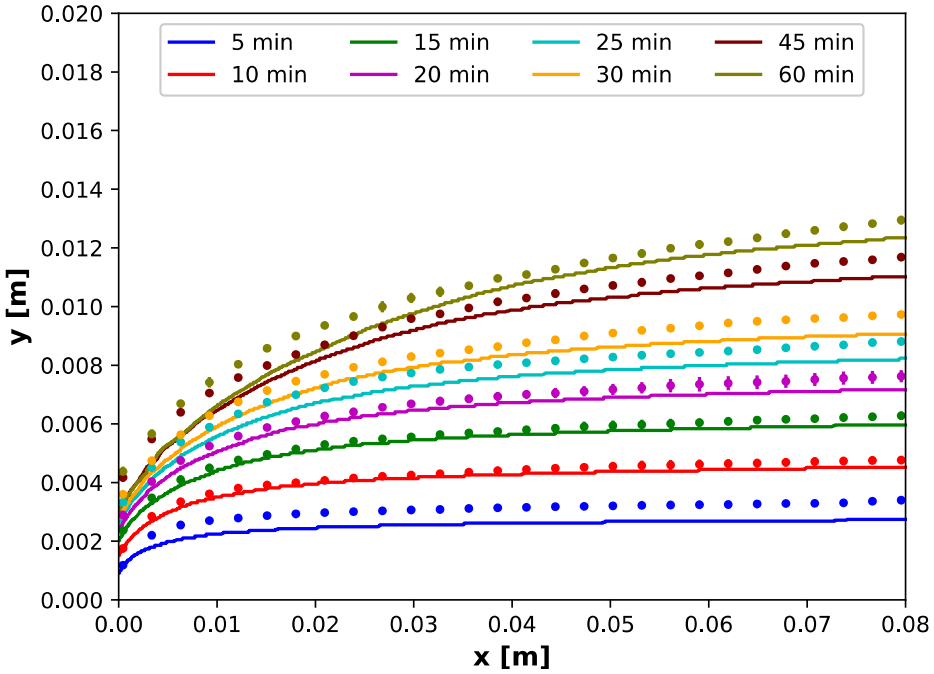

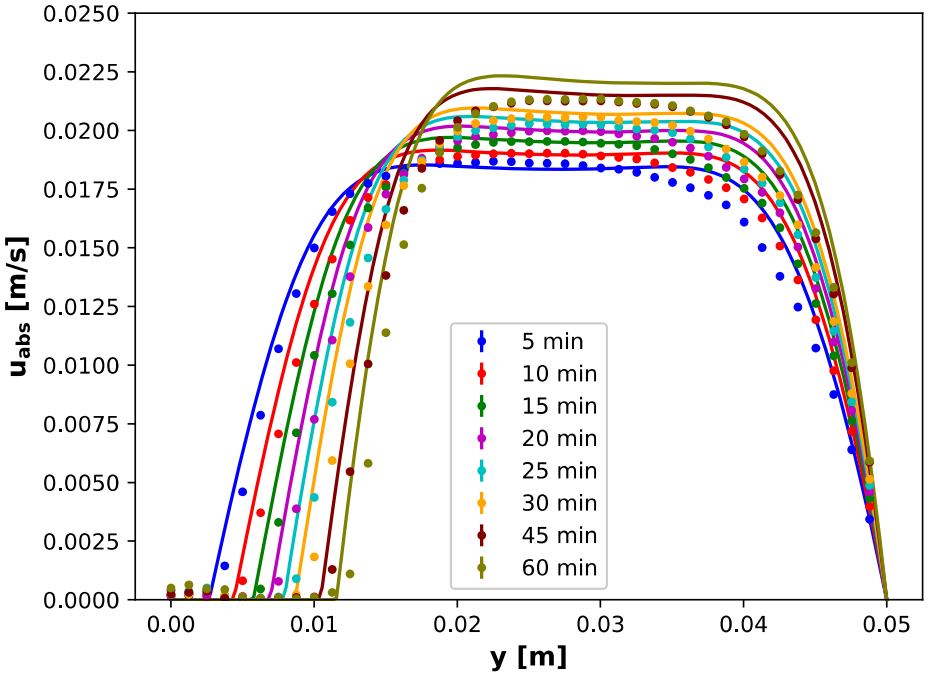

Comparison of experimental transient ice-growth and velocity profiles with the 2D simulation results, for the inlet of the channel.

SAM SAFER

Comparison of Experimental Results with Numerical Simulations (center)

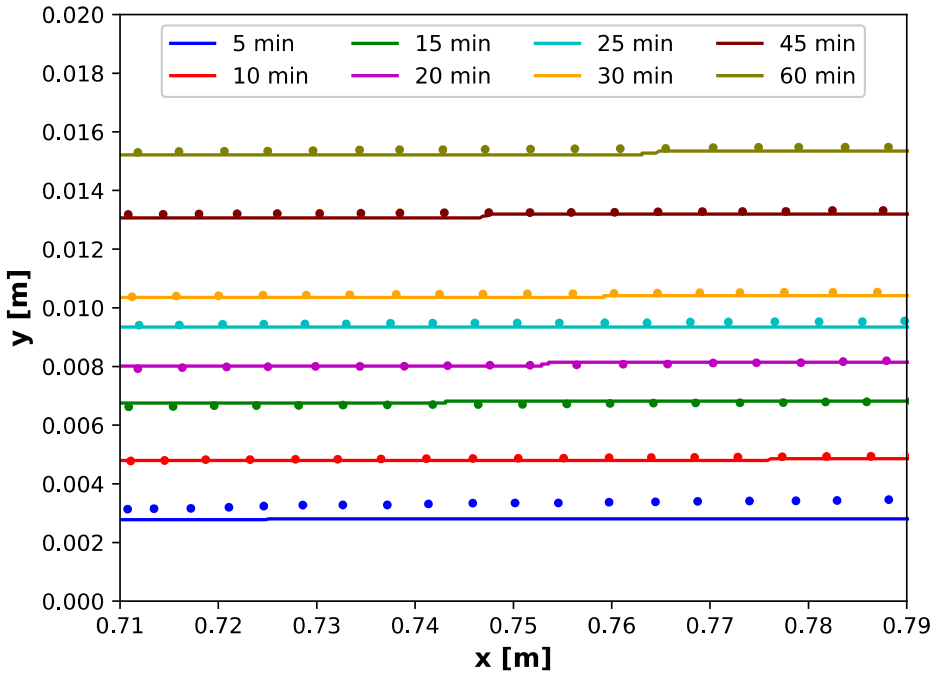

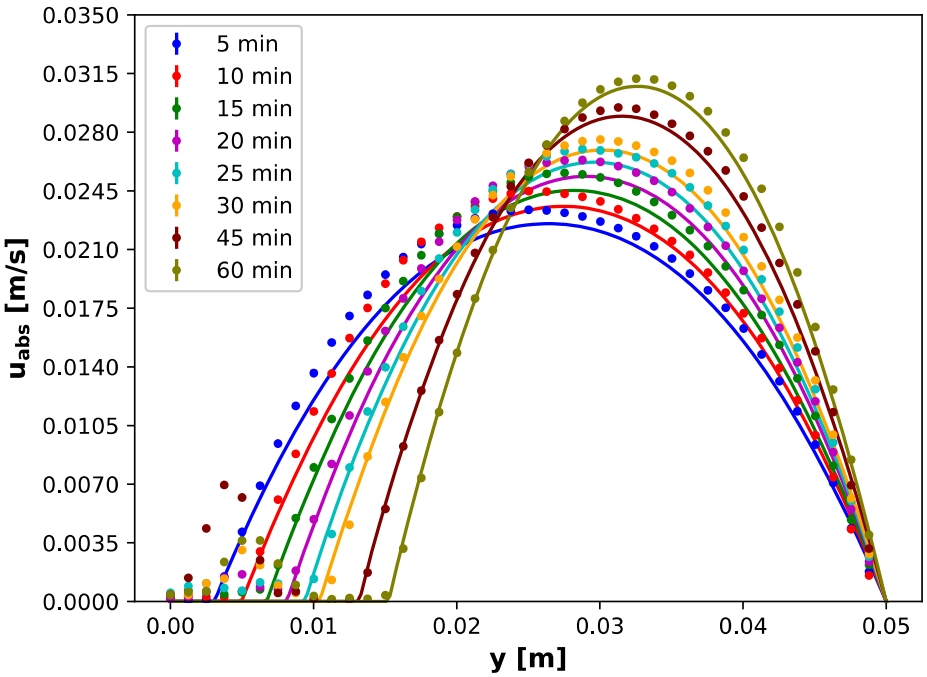

Comparison of experimental transient ice-growth and velocity profiles with the 2D simulation results, for the inlet of the channel.

Conclusions Task 4.2

- A comprehensive and well-described experimental data set was generated for transient freezing in laminar internal flow.
- The onset of ice-formation was found to coincide with a sudden increase of the cold plate temperature, attributed to subcooling effects.
- An overall good agreement was observed between the experimental results and the numerical simulations, with observed discrepancies attributed to the use of a 2D computational domain, the use of constant and isotropic thermophysical properties for each phase, the use of the *Boussinesq* approximation, and possible systematic errors during the experiments.

Dissemination Task 4.2

Deliverables

- D4.2 Design report of ESPRESSO (**completed)**
- D4.3 Validation of tools by detailed basic experiments (**completed)**

Journal papers

- B.J.Kaaks, D.Lathouwers, M.Rohde, J.L. Kloosterman. Transient freezing of water in a square channel: an experimental investigation, *Experimental Heat Transfer* (2023). *Under review*.
- B.J.Kaaks, S. Couweleers, D. Lathouwers, J.L. Kloosterman, M. Rohde. Non-intrusive temperature measurements for transient freezing in laminar internal flow using laser induced fluorescence, *Experimental Thermal and Fluid Science* (2023). *Under review*.

Relevant experimental and numerical data shared in SAMOSAFER Zenodo community.

Task 4.3 Analysis of salt confinement in a large scale MSFR

1. Numerical benchmark for modelling phase-change in the MSFR, modelled after the freeze-valve (together with Mateusz Pater from DTU).
2. Adaptive mesh solver for the MSFR freeze-valve: optimization studies require many simulations and can therefore benefit greatly from a computationally efficient solver.
3. Preliminary numerical investigation of freeze-valve inclination angle (max 45° of clockwise rotation from the original vertical orientation) on the melting time.

A numerical benchmark for modelling phase change in Molten Salt Reactors

- Modelled after the MSFR freeze-plug.
- Step-wise addition of complexity allows pinpointing of sources of discrepancy between the various codes.
- Step 1: Stefan problem with time dependent temperature condition mimicked after the MSFR decay heat transient.
- Step 2: addition of volumetric heating.
- Step 3: addition of conjugate heat transfer (introduces some discrepancies).
- Step 4: addition of natural convection.
- Step 5: addition of forced convection.

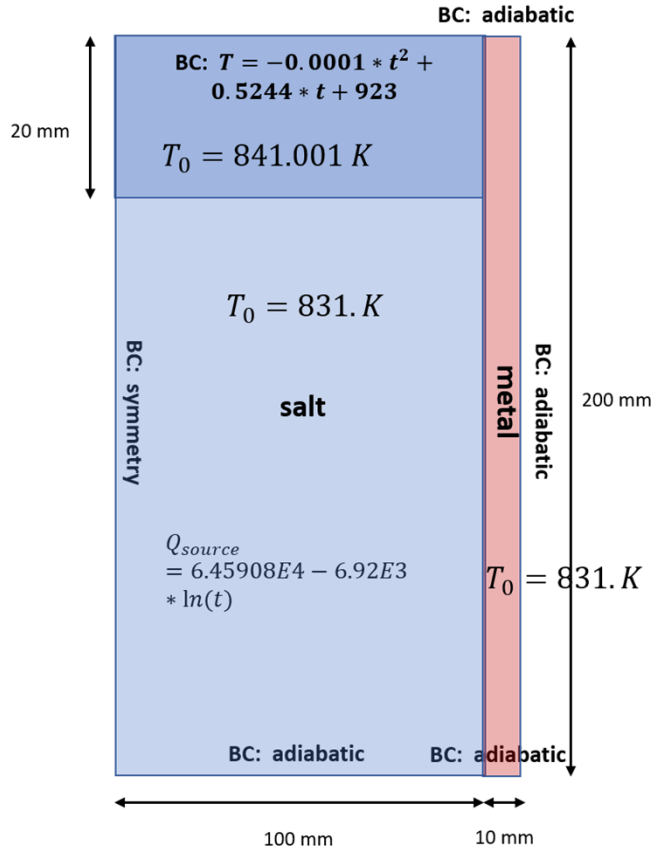

Geometry of the benchmark for stages 3-5.

SAM SAFER

Interface positions

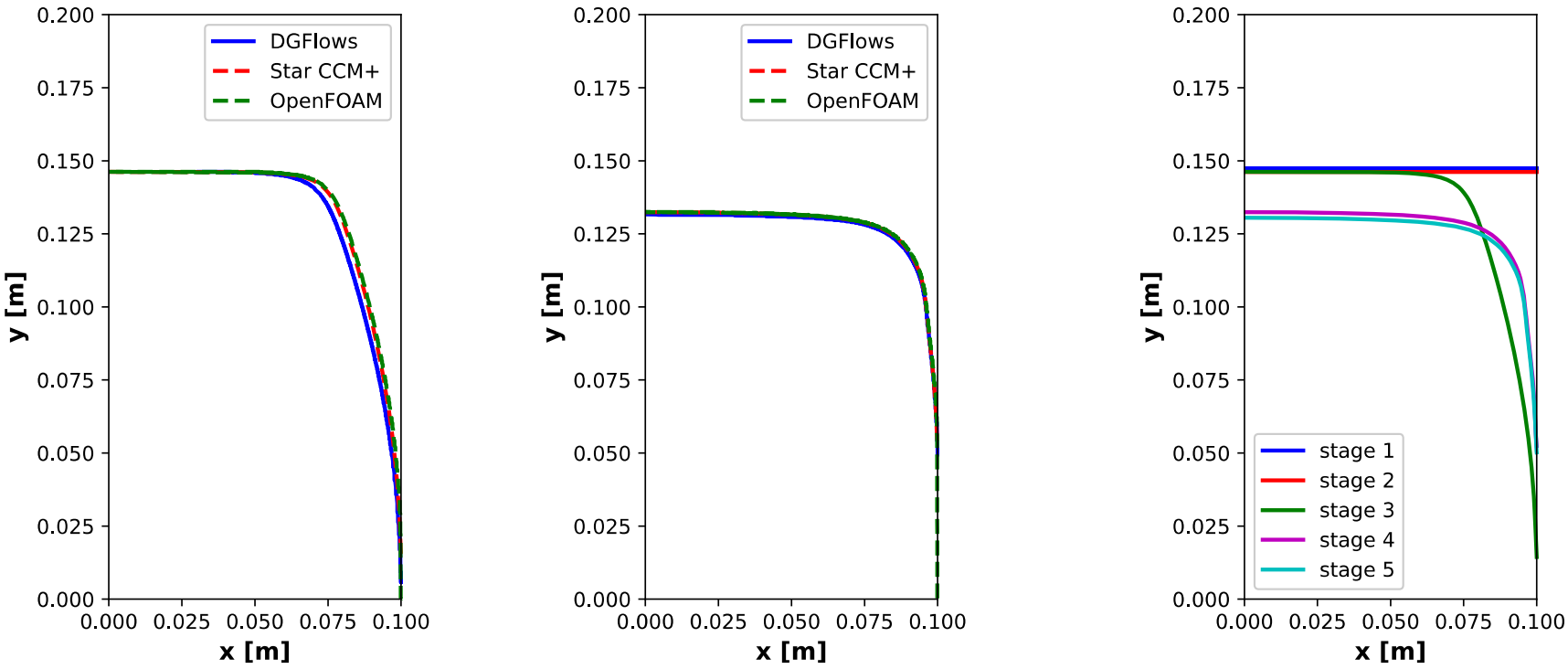

From left to right: agreement between the 3 codes for stage 3 (full geometry including CHT, but no convection) and stage 4 (including natural convection). Comparison in interface position for all 5 cases after 2500s.

Flowfield (stage 4)

- Better agreement between the three codes compared to stage 3, since the heat transfer through the wall is relatively less important. This indicates that coupling between CHT and solid-liquid phase change modelling is a possible source of discrepancy between the codes.
- Two recirculation zones were present: near the top and along the melting front.
- Hot fluid gets transported along the metal wall and flows back down along the solid-liquid interface. This effectively shifts the heat transfer from the metal wall to the top of the plug, prolonging the opening time.

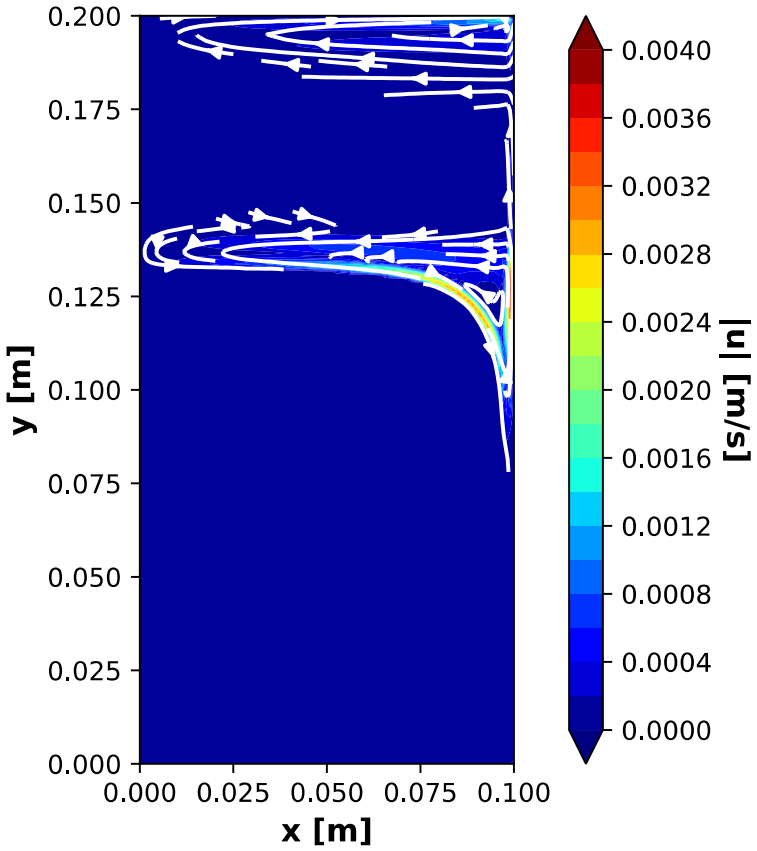

Contour plot of the flow field with the streamlines for stage 4.

AMR simulation of MSFR freeze-valve (single plug decay heat design)

- 2D background mesh of 110×300 elements (axisymmetric boundary conditions), 2 levels of refinement. Compared with solutions on uniform meshes.
- Natural convection included.

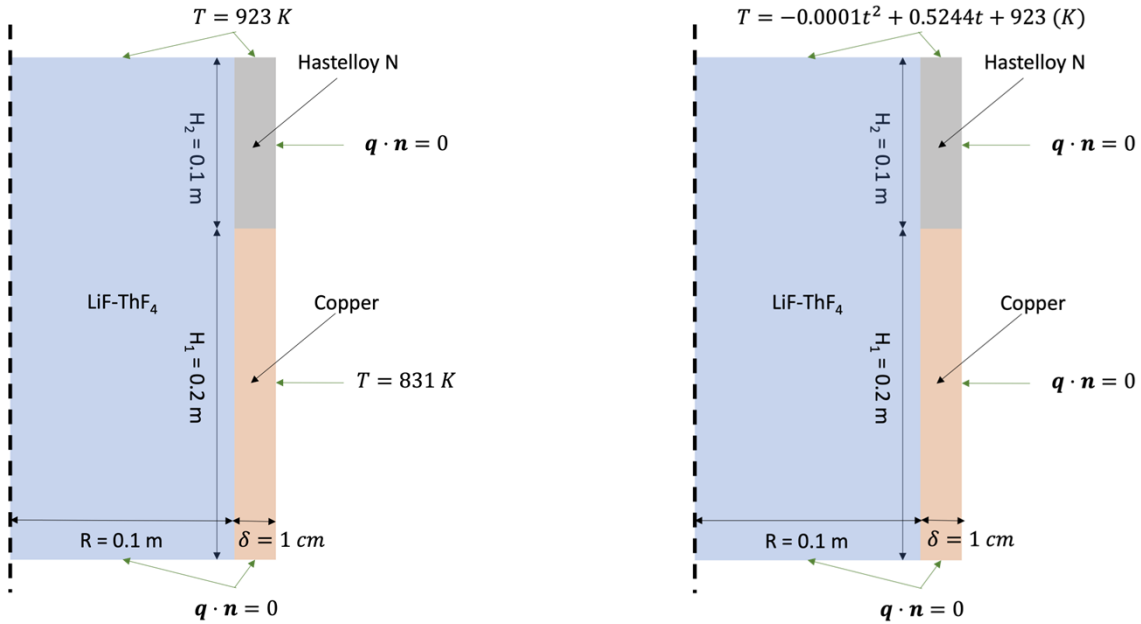

Geometry and boundary conditions of the MSFR freeze-valve (single plug, decay heat design), for both the steady and the transient case.

SAM SAFER

AMR simulation of freeze-plug

- Locally fine resolution obtained using significantly less elements (number of cells doesn't exceed 100,000 compared to 528,000 for the uniform mesh with similar resolution).
- Cells are most significantly refined close to the hastelloy wall, the solid-liquid interface and at the top of the domain, where most of the recirculation takes place.
- Few cells are refined in the copper and the Hastelloy walls, indicating that the largest numerical discretization errors are present in the salt.

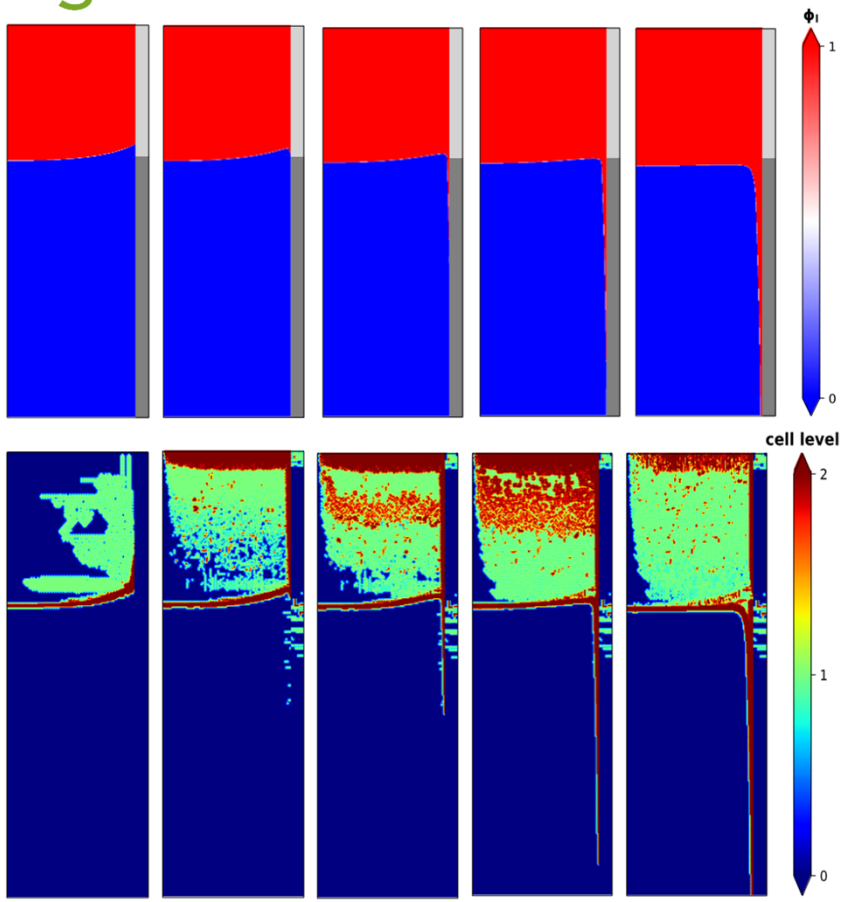

Liquid fraction (top) and cell level (below), at 0 s, 500 s, 1000 s, 1500 s, 2000 s.

SAM SAFER

Prediction of opening time: adaptive vs uniform

- Opening time of the freeze plug sensitive to mesh resolution in the salt near the copper and hastelloy walls.
- Very fine local resolution needed to obtain grid convergent results.
- Excellent agreement obtained between adaptive mesh results and the finest uniform mesh.

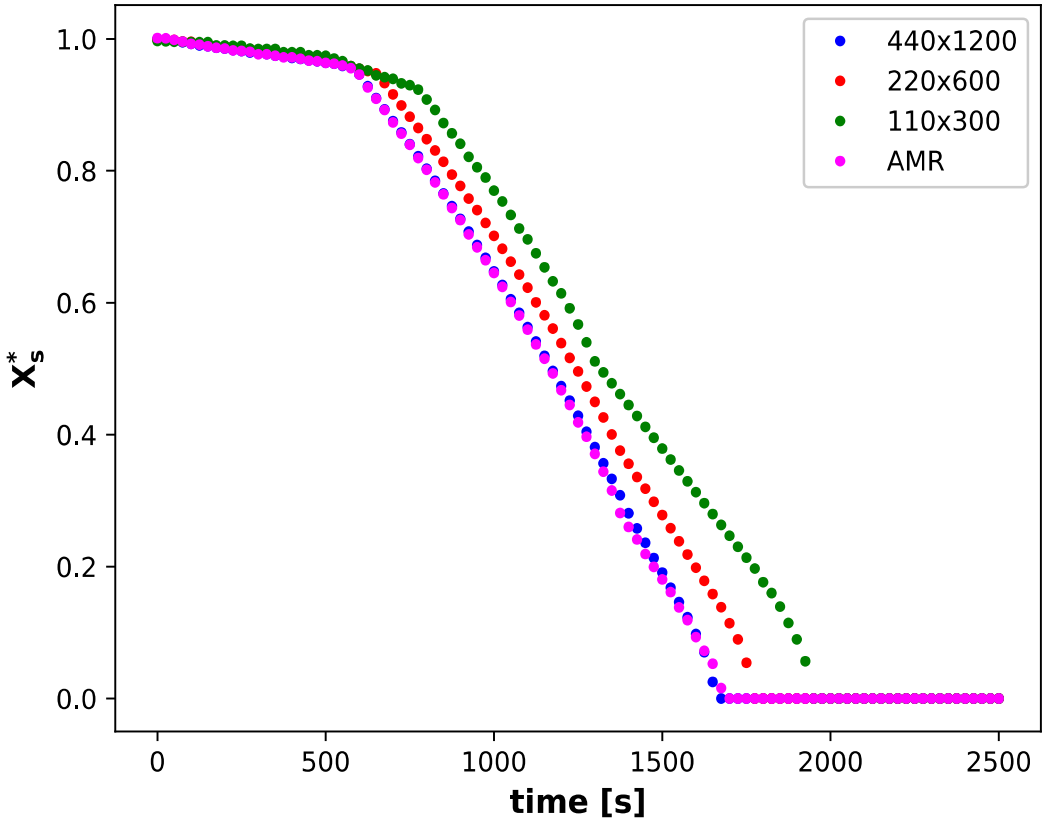

Relative solid fraction of the freeze-plug at the metal wall. Results shown for the adaptive mesh and 3 progressively coarser uniform meshes.

SAM SAFER

Effect of freeze-valve orientation on the melting time (preliminary results)

- 3D uniform mesh of 1.1 million cells.
- By rotating the freeze-plug (in clockwise direction from the original vertical position), the opening time can be drastically shortened.
- For larger opening angles, the stability of the plug can be affected.

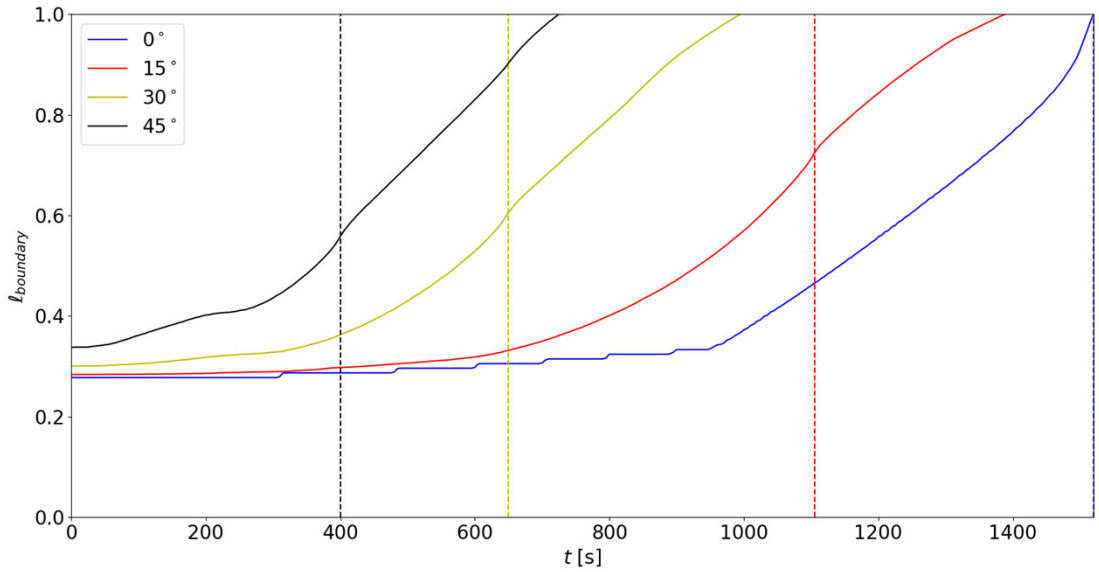

Average liquid fraction at the wall during the transient melting of the plug. Results are shown for four different angles. The dotted lines represent the time at which the freeze plug detaches from the left wall.

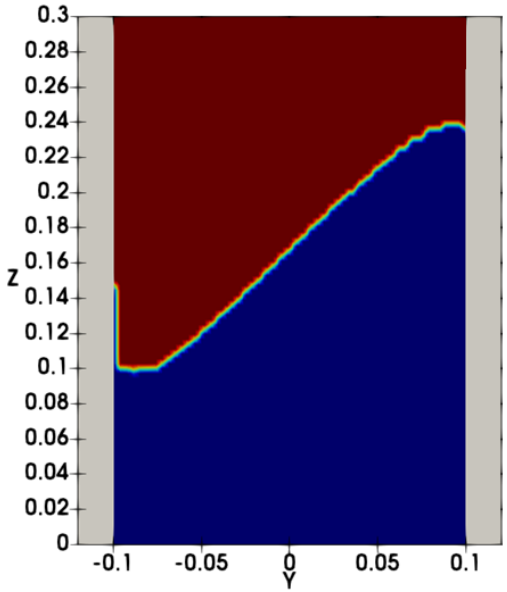

Steady-state freeze plug shape for a clockwise rotation of 45º.

SAM SAFER

Conclusions Task 4.3

- A difference in CHT modelling approach can lead to a different outcome of the predicted melting front positions.
- Natural convection has a non-negligible effect on the freeze-valve melting transient (even for a vertical orientation of the plug).
- Freeze-valve simulations are sensitive to the local resolution, especially in the near-wall region. AMR can be beneficial for performing mesh-converged simulations at affordable computational cost.
- Preliminary results show that a significant reduction in opening time can be obtained by changing the freeze-valve orientation from vertical to inclined. However, this may affect the stability of the plug under steady-state conditions.

Dissemination Task 4.3

Deliverables

- D4.4 Salt confinement and thermal load prediction (**work in progress)**

Journal papers

- M. Pater, B.J. Kaaks, B. Lauritzen and D. Lathouwers. A numerical benchmark for modelling phase change in molten salt reactors, *Annals of Nuclear Energy* 194, 110093 (2023). doi:10.1016/j.anucene.2023.110093.

Relevant numerical data sets shared in SAMOSAFER Zenodo community.

WP4: decay heat in the Emergency Draining System

Thibault Le Meute and Juliette Plantier

Under the supervision of Frédéric Bertrand, Axel Laureau, Elsa Merle, Nathalie Seiler, Daniel Heuer

Decay heat in the Emergency Draining System: outline

1 – Emergency Draining System (EDS)

- Presentation
- Size and design

2 – Residual power

- Computation and emitted particles
- Transport of particles in the EDT (Emergency Draining Tank)

3 – Heat removal

- Case presentation
- Pure conduction
- Pure convection

SAM SAFER

Emergency Draining System (EDS)

Presentation

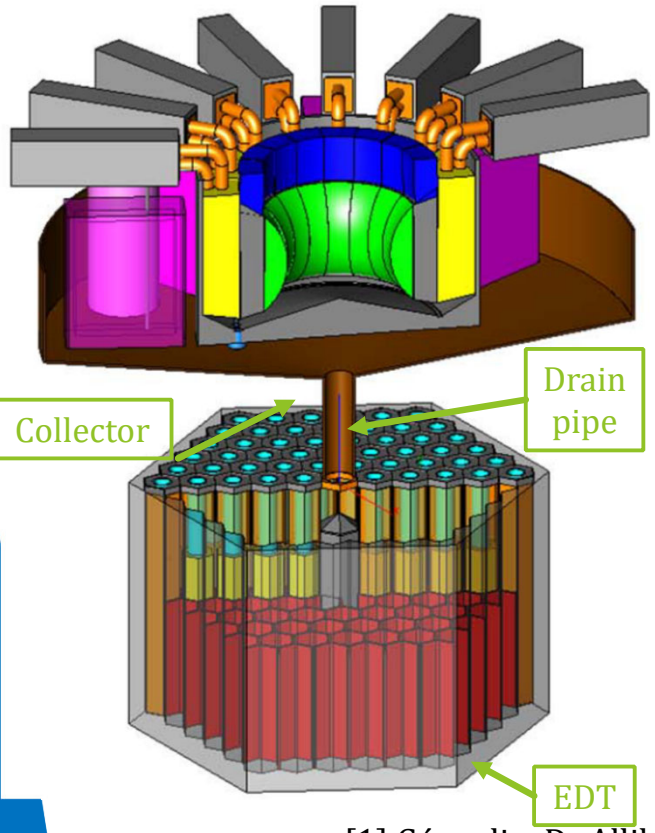

- Emergency Draining System (EDS):
  - Collector
  - Drain pipe
  - Emergency Draining Tank (EDT)
- Aims at:
  - Sub critical geometry of the fuel salt
  - Remove the residual power (aim of this work)

Hexagonal geometry in the EDT:

- Maximize the surface of the fuel in contact with the structure
- Minimize the compacity

Sub critical geometry of the fuel salt [1]

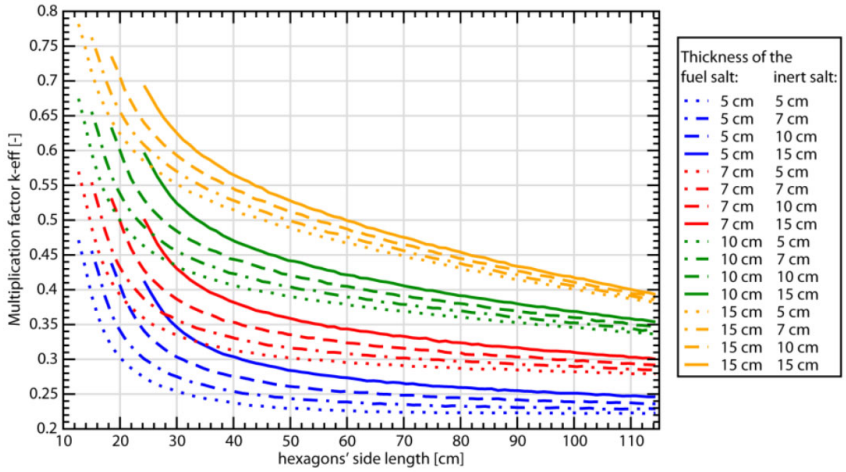

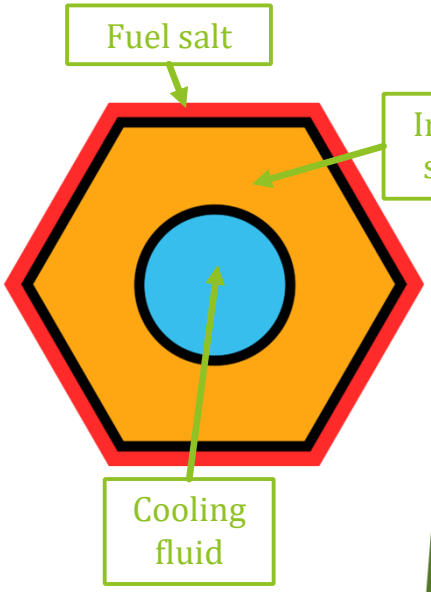

[1] Gérardin, D., Allibert, M. & al.Design evolutions of the molten salt fast reactor.

SAMOSAFER

SAM SAFER

Residual power

Computation and emitted particles

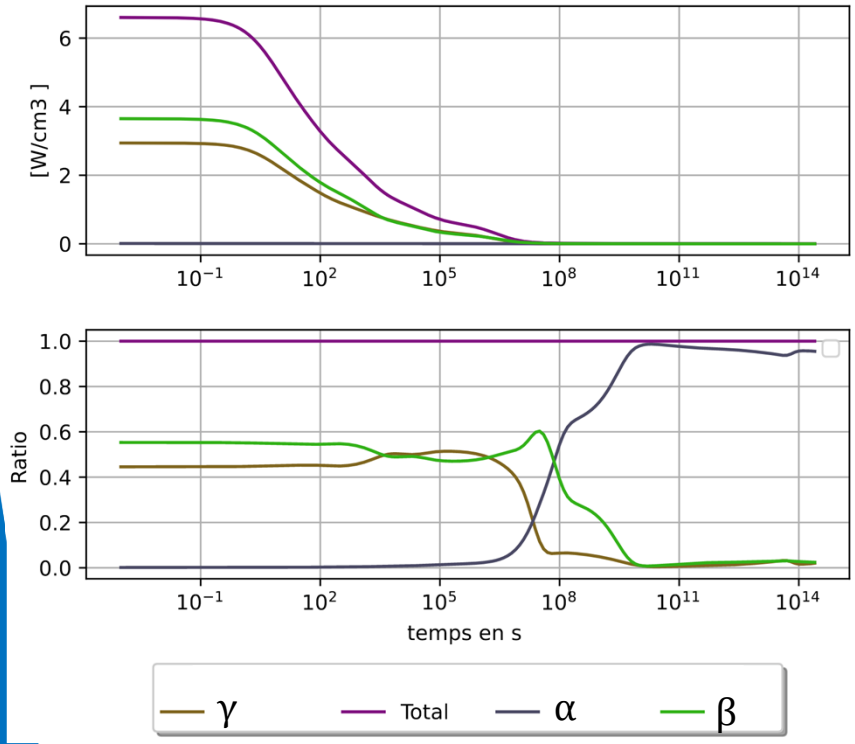

- Decay of the different nuclei:
  - α, β and γ deexcitations
- Use of the computation tool ECI (developed at CNRS/LPSC)

$$N_n(t) = N_1(0) \times \left(\prod_{i=1}^{n-1} \lambda_i \right) \times \sum_{i=1}^{n} \frac{e^{-\lambda_i t}}{\prod_{j=1, j \neq i}^{n} (\lambda_j - \lambda_i)}$$

Depends strongly on the evolution state of the fuel salt
Here, reference MSFR at steady state

Transport of particle in the EDT

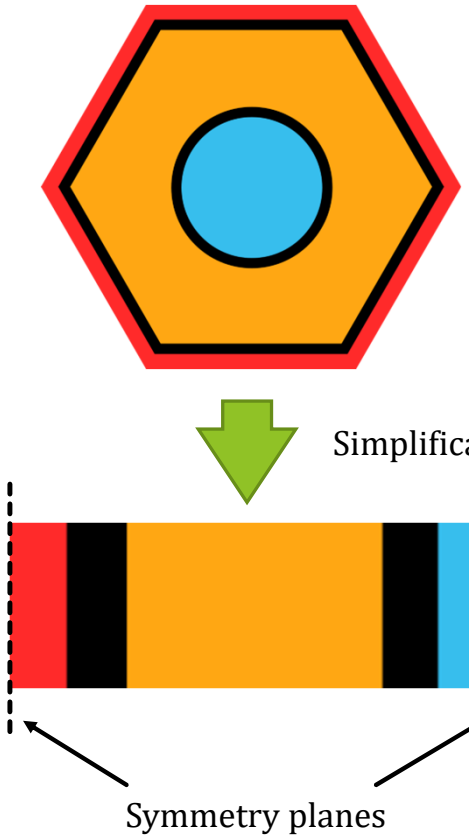

- α: Heavy particle, stop immediately in the fuel salt
- β: Light and charged particle, can travel in the salt
- γ: No mass and uncharged particle, can travel far in the structure

→ β: Light and charged particle, can travel in the salt
  - Fuel salt has a high stopping power
  - β of 6 MeV travel less than 1 µm in the fuel salt
  - Due to high charge number of some of the nuclei

→ γ: No mass and uncharged particle, can travel far in the structure
  - Modelling thank to the stochastic code OpenMC
  - ECI provides γ spectrum

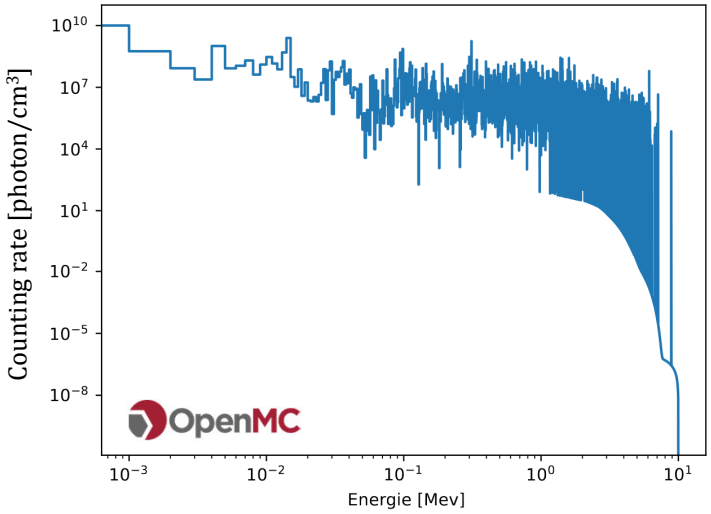

SAM SAFER

Transport of particle in the EDT

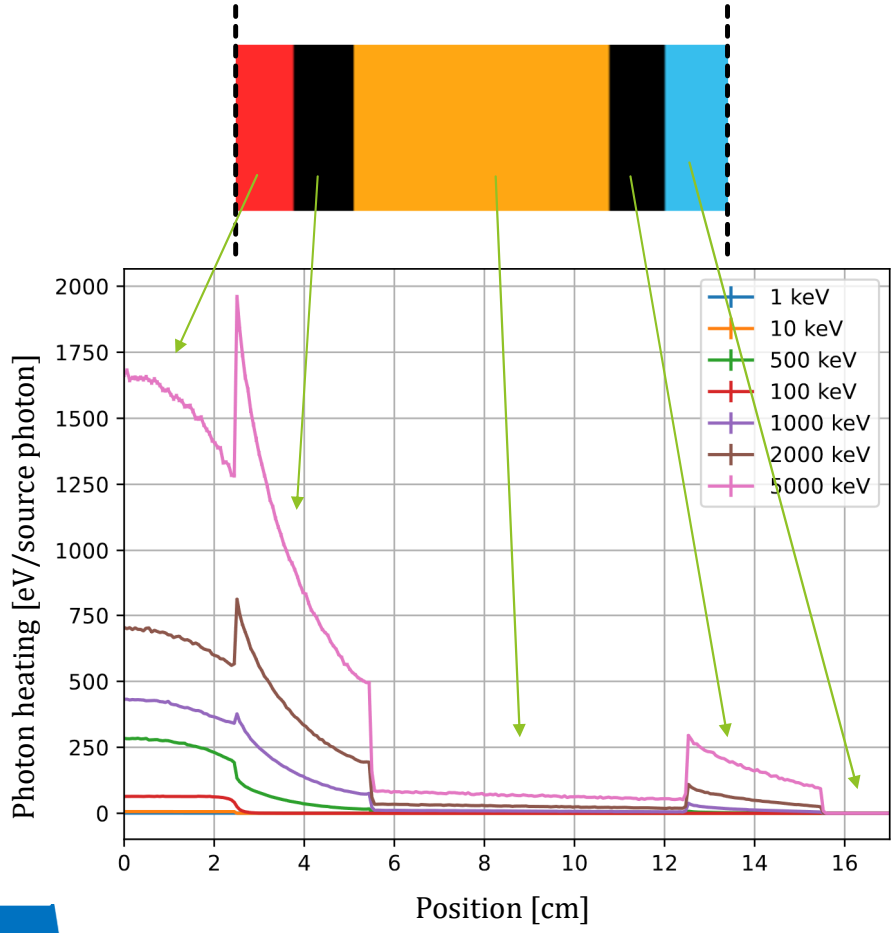

Photon counting rate coupled with the OpenMC calculation to estimate the power deposit in each material of the EDT

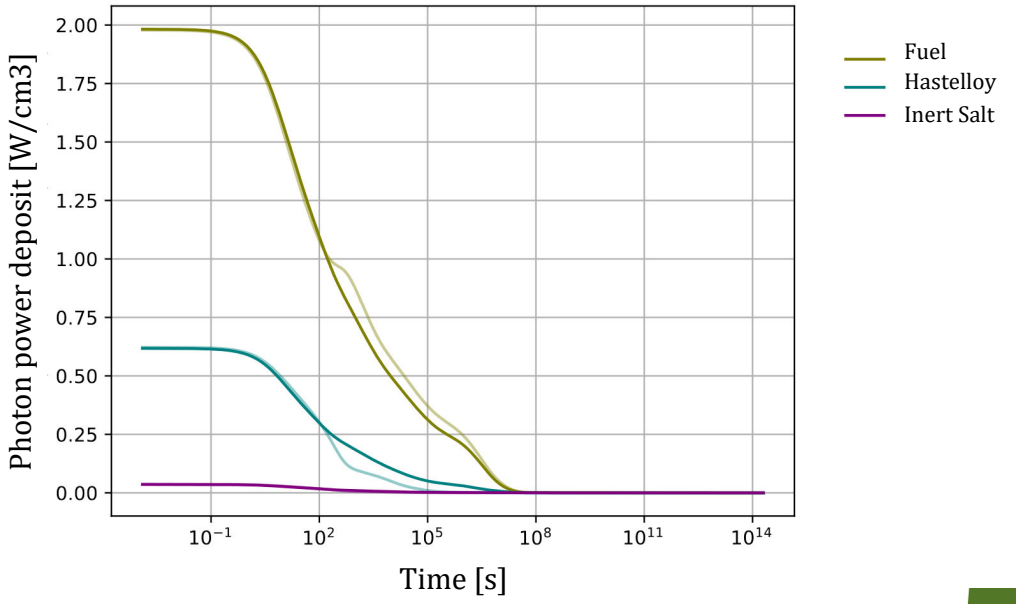

SAM SAFER

Heat removal

Case presentation

- Modelling the heat transfer in the EDT with the OpenFOAM code
- Monitoring the evolution of the maximal temperature calculated in the structure
- Velocity of the cooling fluid distribution mapped on the outlet and magnitude define by user

<u>Pure convection:</u>

- Don't take into account melting
- Optimistic situation for safety

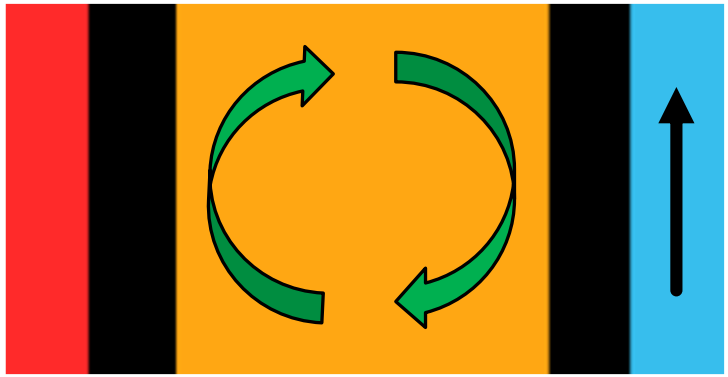

<u>Pure conduction:</u>

- Don't take into account melting
- Penalizing situation for safety

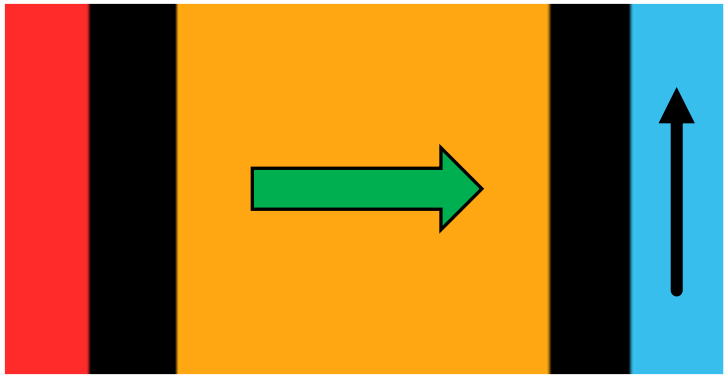

SAM SAFER

Case 1: Pure conduction

- Inert salt has a really low thermal conduction = thermal insulator
- When the amount of inert salt decreases, the maximal temperature calculation decreases
- When the hastelloy thickness increases, the maximal temperature in the fuel salt decreases: due to the thermal conductivity of the hastelloy and its heat capacity

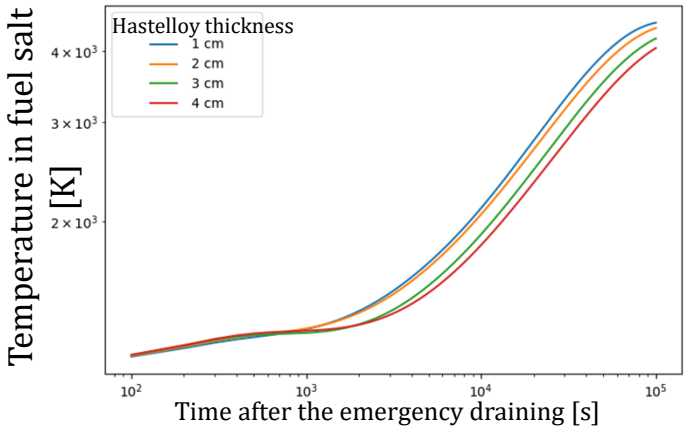

15 cm of inert salt

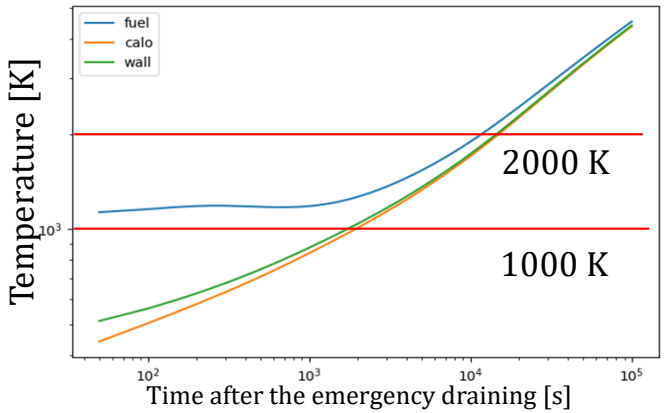

7 cm of inert salt

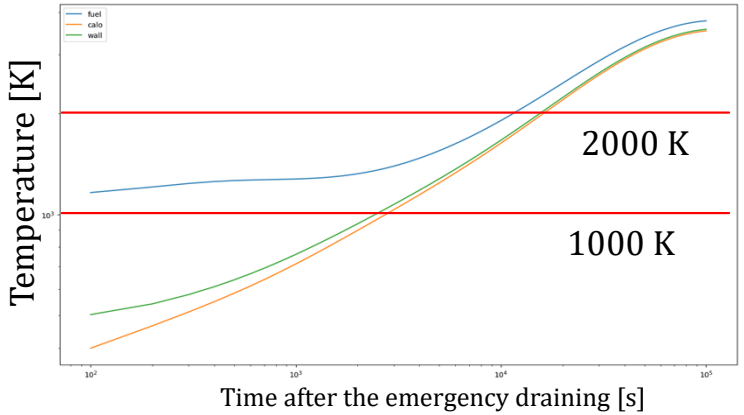

SAM SAFER

Case 2: Pure convection

- Natural convection is a good thermal bridge between fuel salt and cooling fluid
- When the amount of inert salt increases, the maximal temperature calculation decreases (opposite way than the conduction)
- When the hastelloy thickness increases, the maximal temperature in the fuel salt decreases: due to the thermal conductivity of the hastelloy and its heat capacity

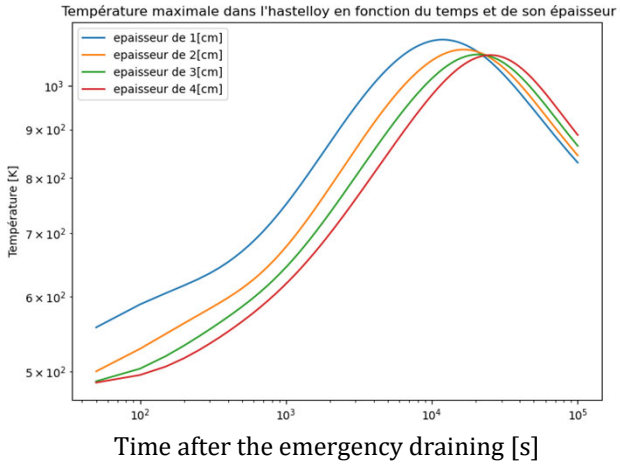

15 cm of inert salt

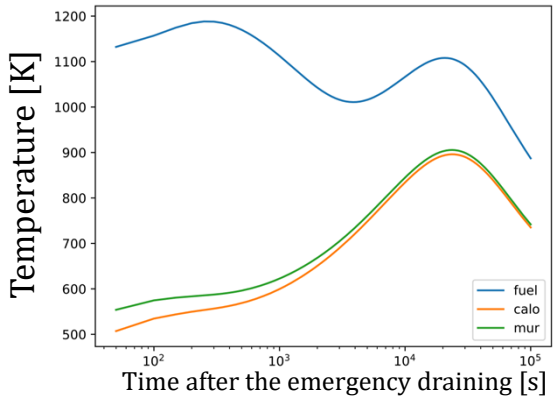

7 cm of inert salt

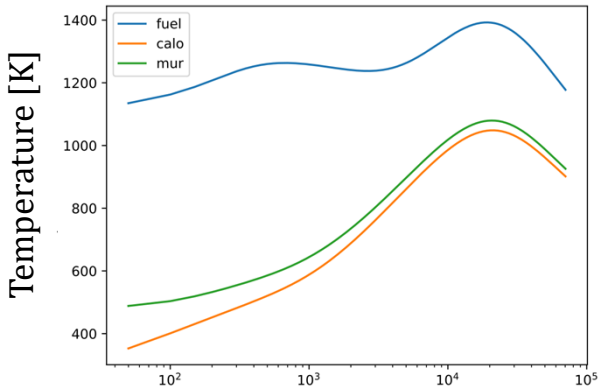

SAM SAFER

SAM SAFER

Conclusion and perspectives

Conclusion and perspectives

Methodology

- Computation of the decay heat from a fuel salt composition (ECI code)
  - From all the different particles (α, β, γ)
  - Compute the γ emission spectrum
- Compute the γ power deposition in each cell
- Compute the heat transfer

Perspectives: Optimization

- Optimize the size of each part of the EDT to guarantee the material durability during accident transient
- Study of the geometry (fins in the inert salt may help transfer heat and fuse the inert salt?)
- Optimization of the heat exchangers between the containment and the outside air to cool the EDT

Perspectives: Computations

- Study the impact of the fuel salt treatment, and the position in evolution on the decay heat
- Compute the γ energy deposit in the hexagonal geometry of the EDT
- Take into account the melting energy of the inert salt in the computation
- Take into account the melting of the inert salt and the real transient between conduction and convection
- Compute the air flow in natural convection in the reactor containment and outside

Thank you for your attention

Analysis of salt confinement in a large scale MSFR: thermo-mechanical analysis

Stefano Lorenzi, Antonio Cammi, Sophie Deanesi, Davide Pizzocri (PoliMi)

SAMOSAFER Final Meeting & Exploitation Workshop
Avignon, France, 28-30 November, 2023

Thermo-mechanical issues of the confinement

Objective:

Perform a preliminary thermo-mechanical analysis of the reactor containment

Approach:

- Definition of material properties and behavioral models (Hastelloy N)
- Map of thermal load, pressure and fluence on the reactor confinement (OF multiphysics solver)
- Thermo-mechanical analysis

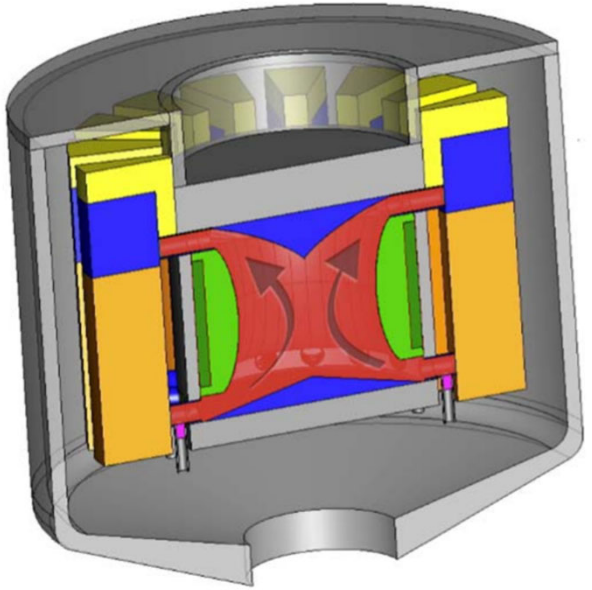

Definition of material properties

- Focus on Hastelloy N
- Thermal properties and mechanical
- Thermal and irradiation creep (included in the analysis)
- Void swelling and Helium embrittlement (require additional investigation)
- Properties collected in Abaqus library and available for use

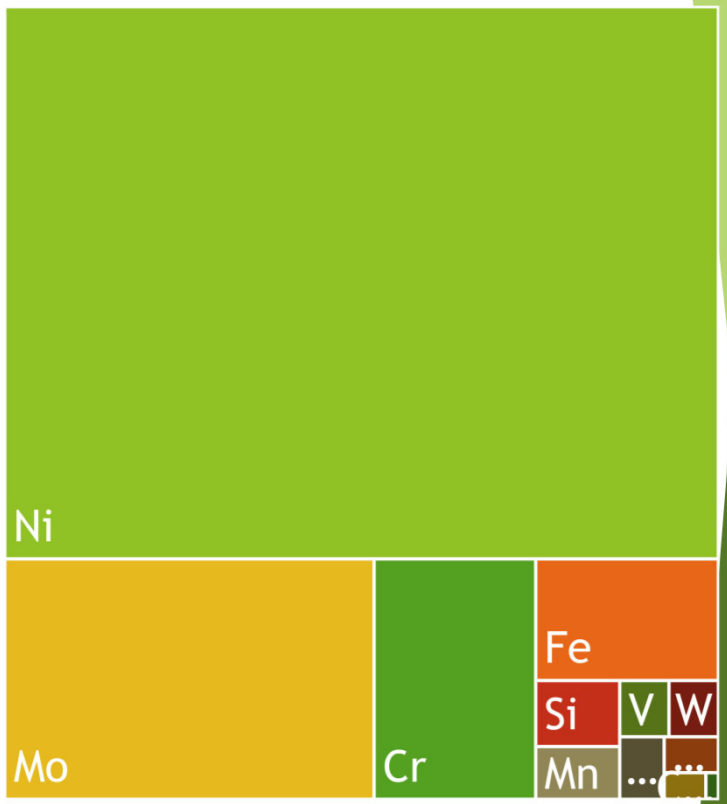

SAM SAFER

Thermal expansion coefficient & Thermal conductivity

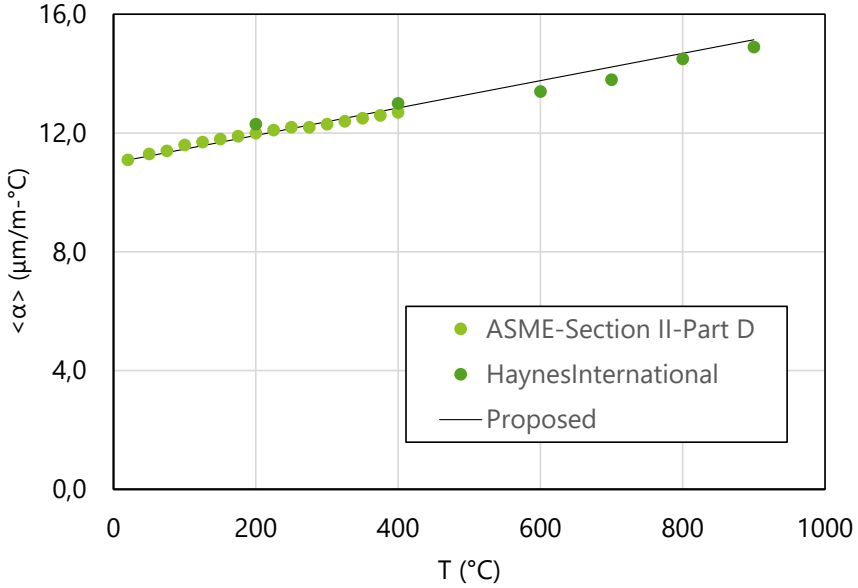

$$< \alpha > \left(\frac{\mu m}{m\ °C}\right) = 0.0046\ T\ (°C) + 11$$

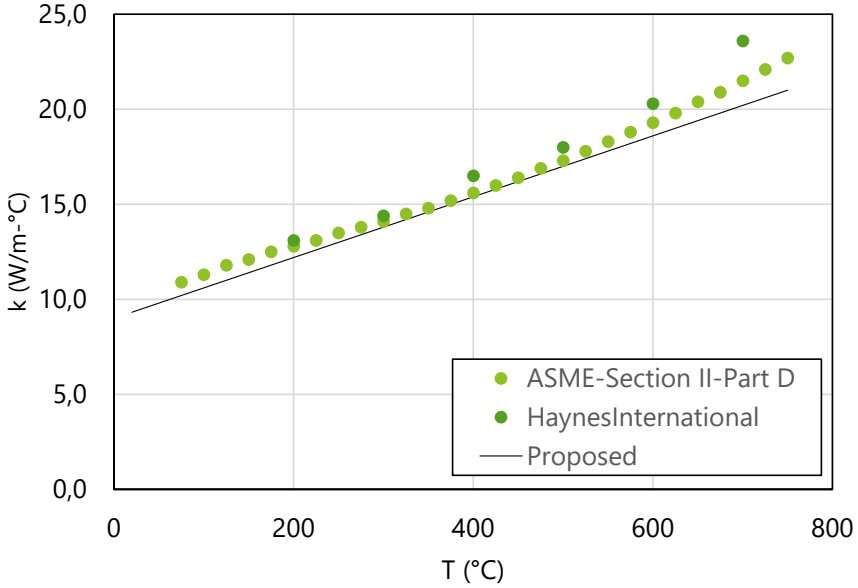

$$k\left(\frac{W}{m\ °C}\right) = 0.016\ T\ (°C) + 9$$

SAM SAFER

Young's modulus & Poisson ratio

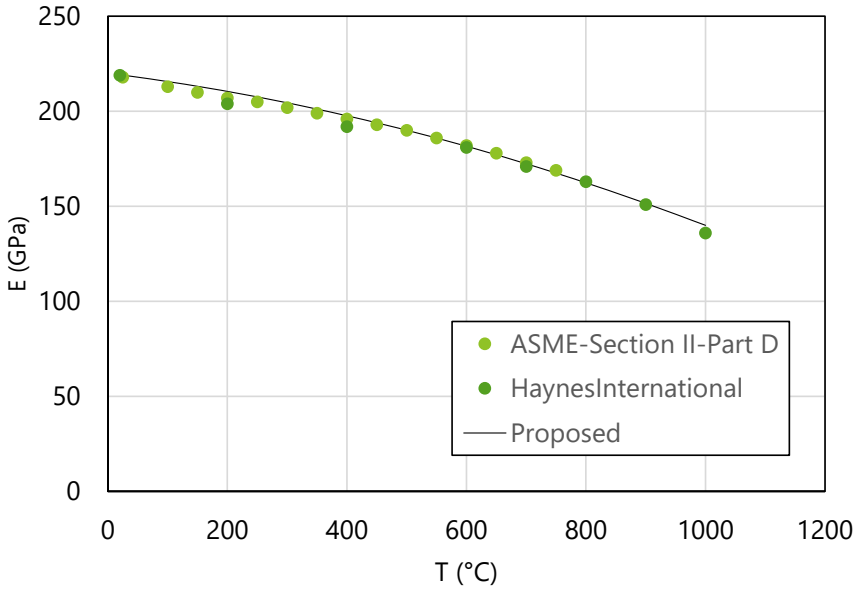

$$E(\text{GPa}) = -4\ 10^{-5}\ T(°\text{C})^2 - 4\ 10^{-2} T(°\text{C}) + 220$$

$$\nu(/) = 0.31$$

$$\sigma_{\text{th}} \propto \frac{< \alpha > E}{(1-\nu)k}$$

$$\sigma_{\text{th}} \approx 3.5 \frac{\text{MPa}}{°\text{C}}\ @650°\text{C}$$

SAM SAFER

Thermal creep

- Behaviour in salt comparable to behaviour in air
- Irradiation effect is minimal even at high dpa

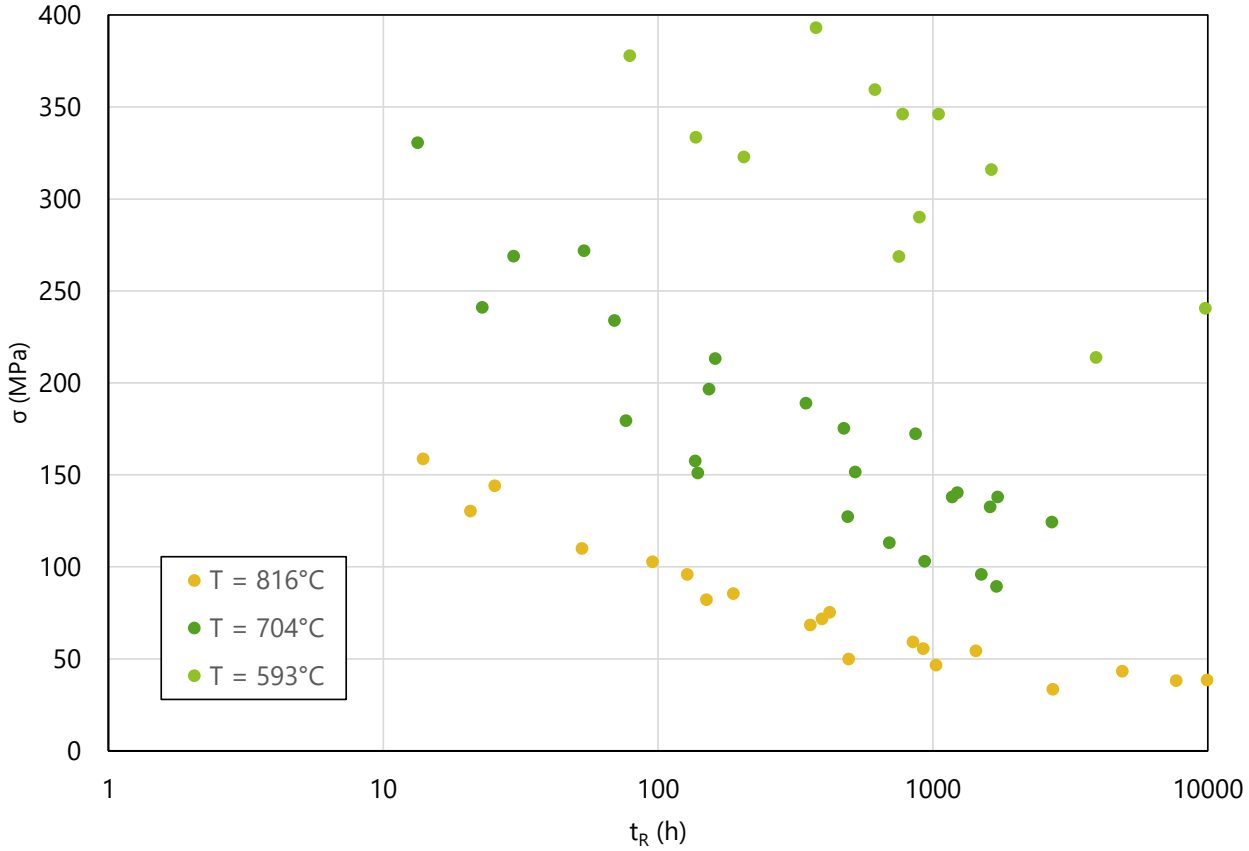

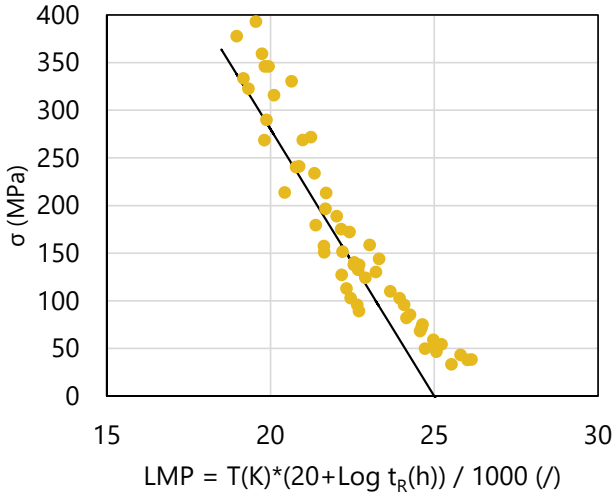

$$\mathrm{LMP} = T(\mathrm{K})[20 + \mathrm{Log}\, \mathrm{t_R(h)}]$$

$$\sigma\ (\mathrm{MPa}) = -56\ \mathrm{LMP} + 1400$$

$$\sigma\ (\mathrm{MPa}) = \mathrm{A}\ \exp(-\mathrm{b}\ \mathrm{LMP})$$

SAM SAFER

Multiphysics calculations for thermal load mapping

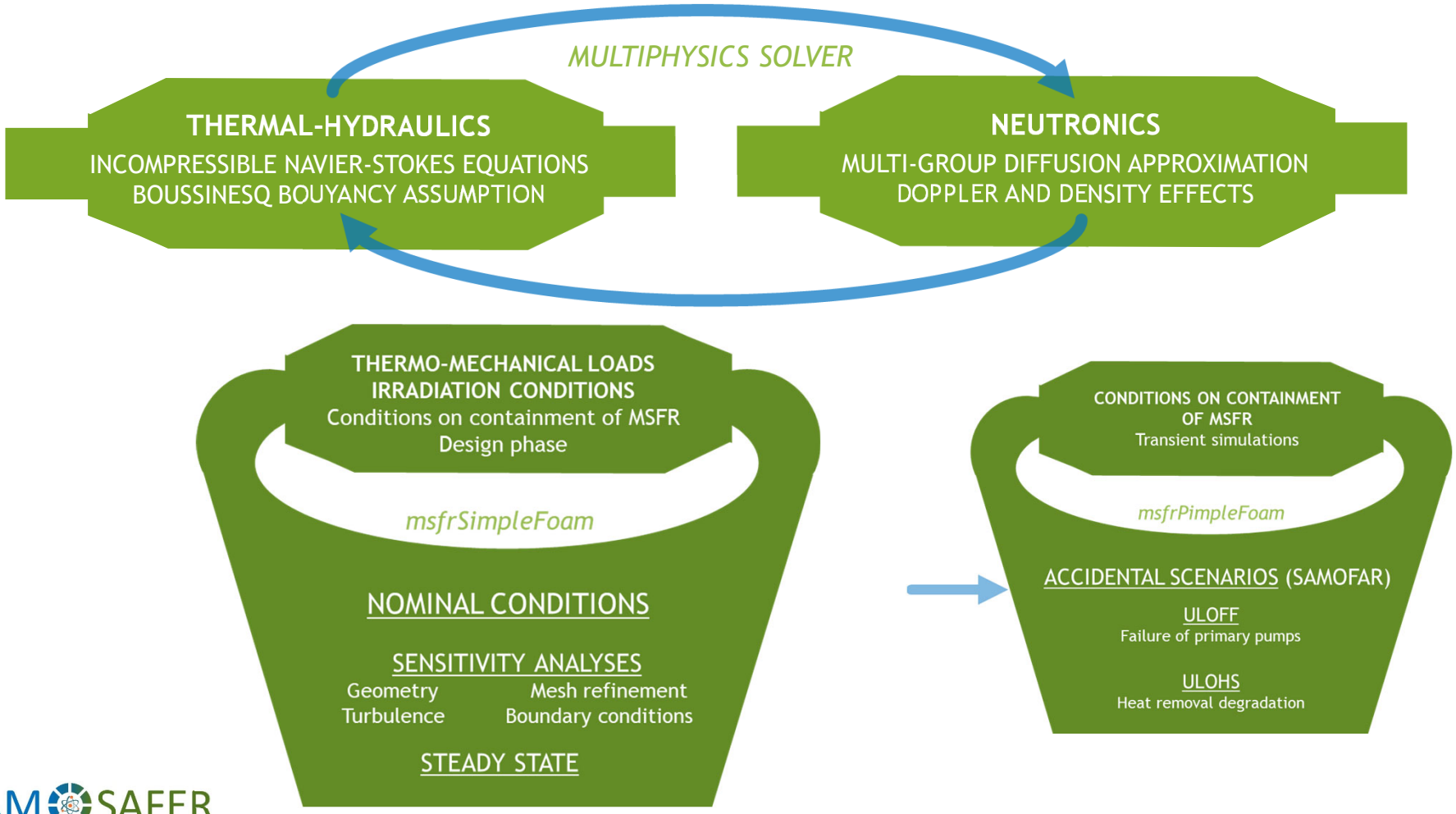

SAM SAFER

Geometry

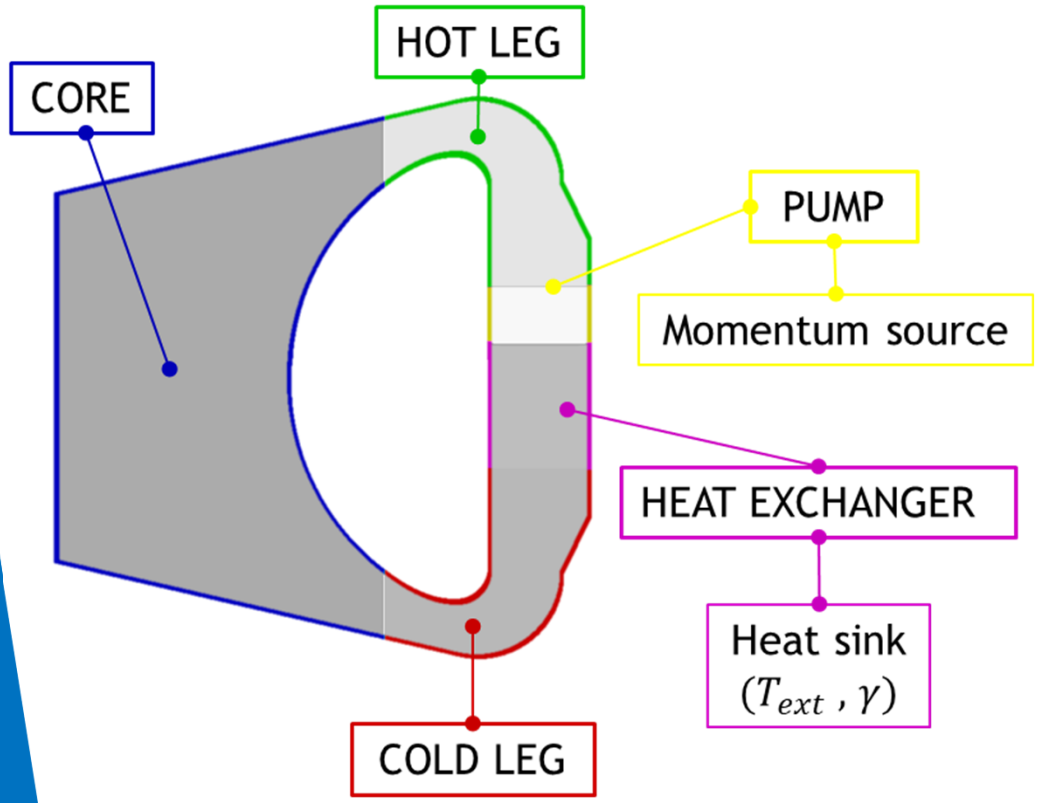

OPERATIONAL PARAMETERS

Nominal power $Q = 3000\ \mathrm{MW_{th}}$

Volumetric flowrate $\dot{V} = 4.5\,\frac{m^3}{s}$

Minimum temperature at core inlet $T_{min,inlet} = 923\ \mathrm{K}$

SENSITIVITY ANALYSES

GEOMETRY

TURBULENCE MODEL

NEUTRONIC BOUNDARY CONDITIONS

PRE-IMPLEMENTED SOURCE

MESH REFINEMENT

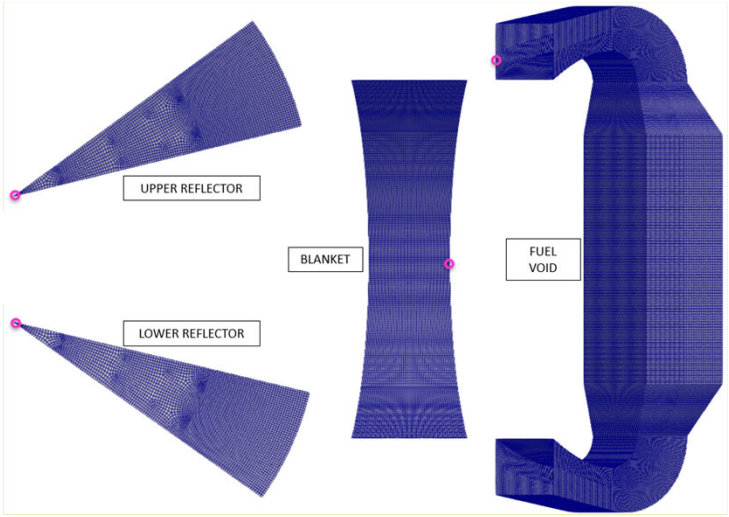

SAM SAFER

Mechanical load

SAM SAFER

Thermal load

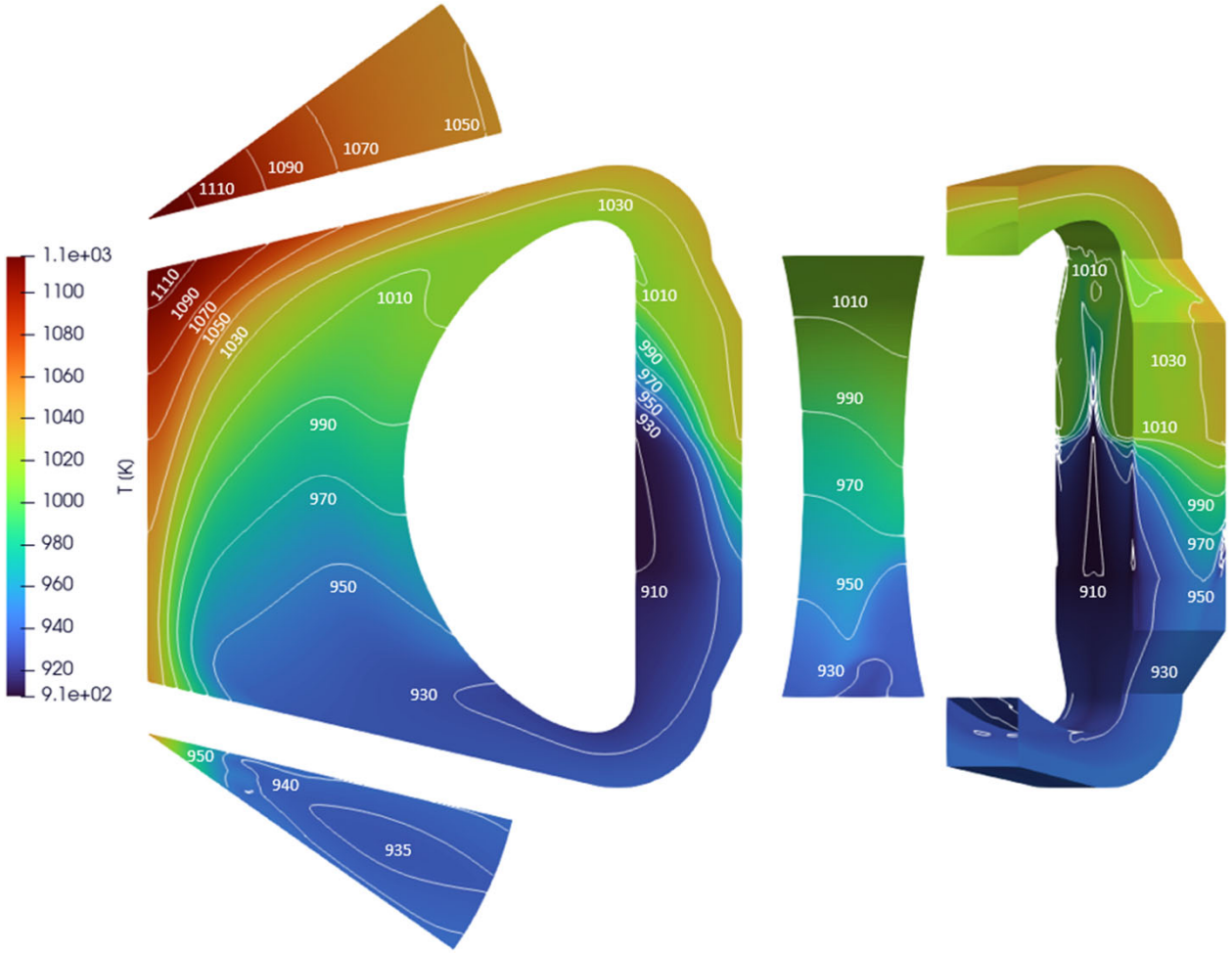

SAM SAFER

ULOHS

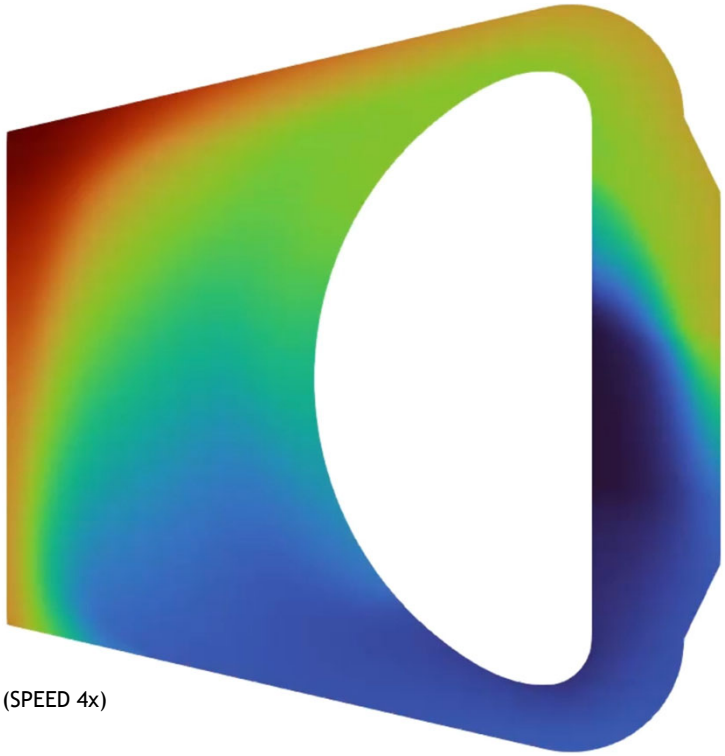

(SPEED 4x)

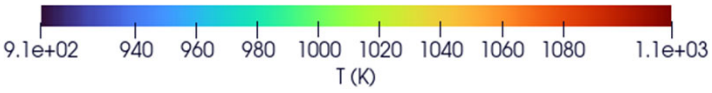

REALISTIC SCENARIO

Exponential increase of intermediate salt temperature $\uparrow T_{ext}$

Exponential drop of global heat transfer coefficient $\downarrow \gamma$

VOLUMETRIC FLOWRATE

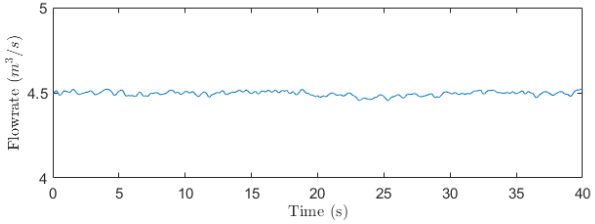

TOTAL POWER

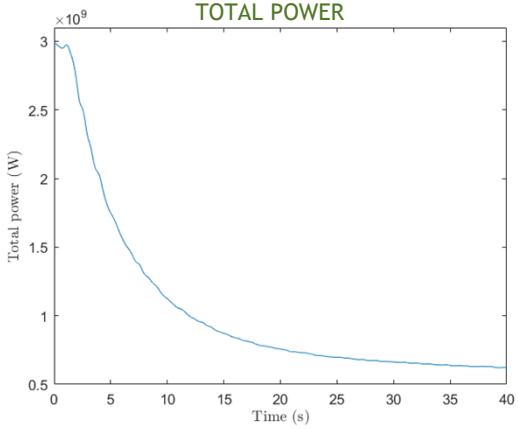

MEAN TEMPERATURE

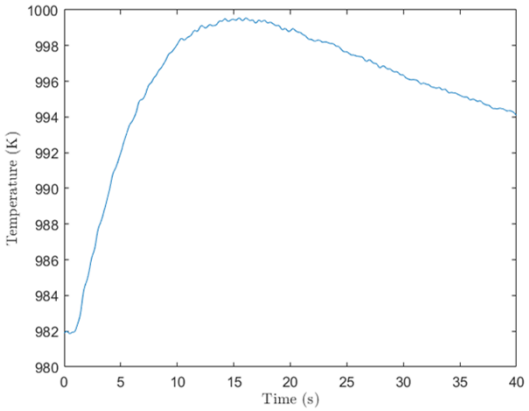

SAM SAFER

ULOFF

$$f(t) = f_0 e^{-t/5}$$

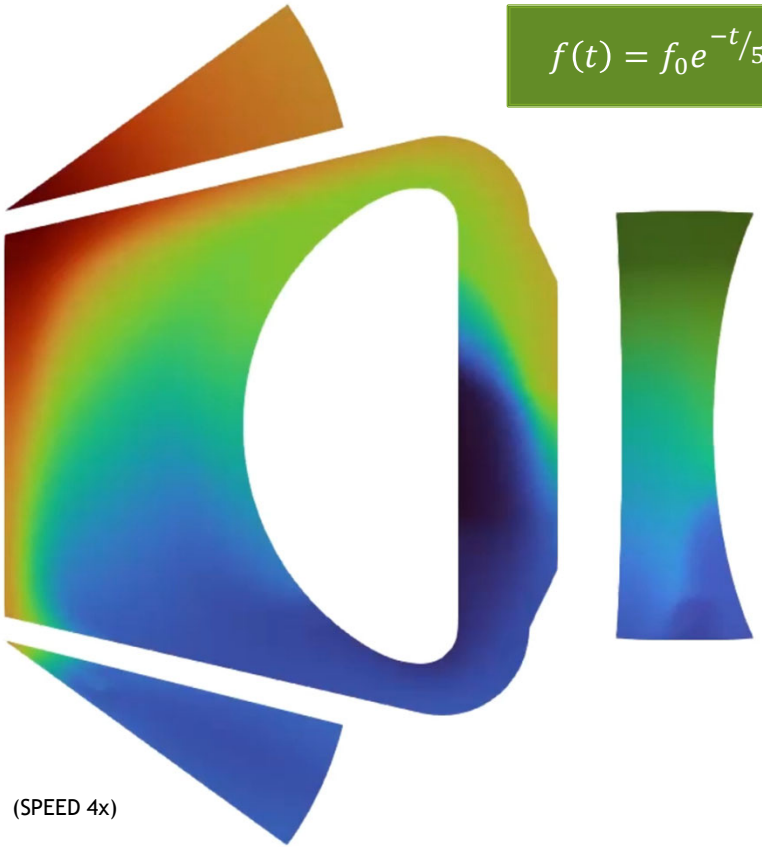

(SPEED 4x)

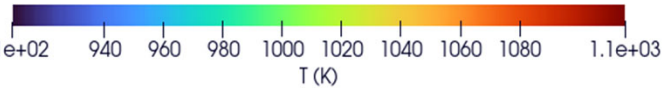

VOLUMETRIC FLOWRATE

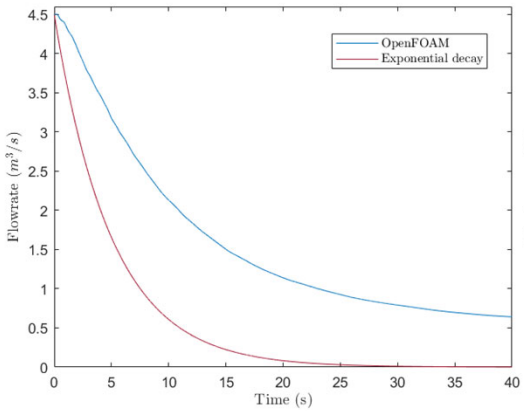

TOTAL POWER

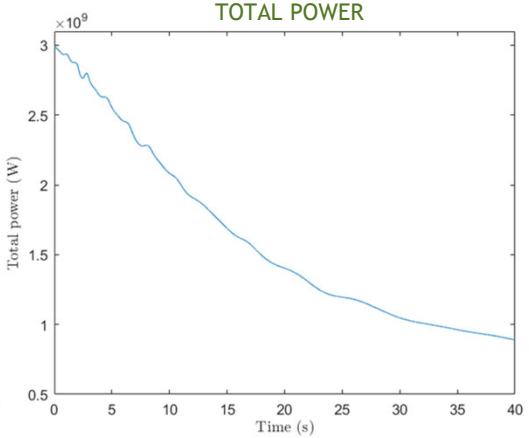

MEAN TEMPERATURE

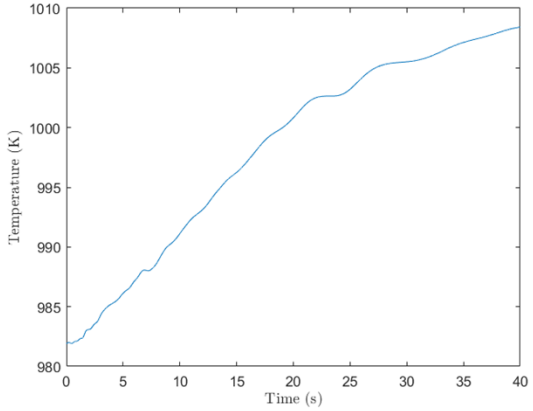

t = 0 s

t = 40 s

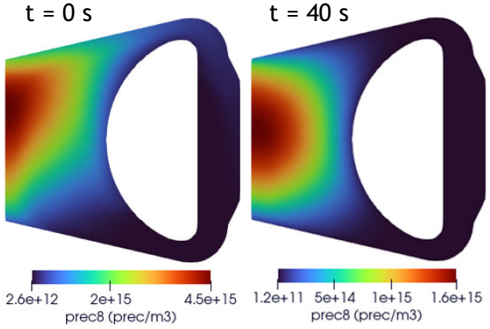

SAM SAFER

Thermo-mechanical analysis of the confinement

- Identification of design conditions (connection with multiphysics calculations)
- Construction of mechanical model (including first hypothesis of constrains)
- Analysis in normal operation
- Thermal creep verification in critical sections

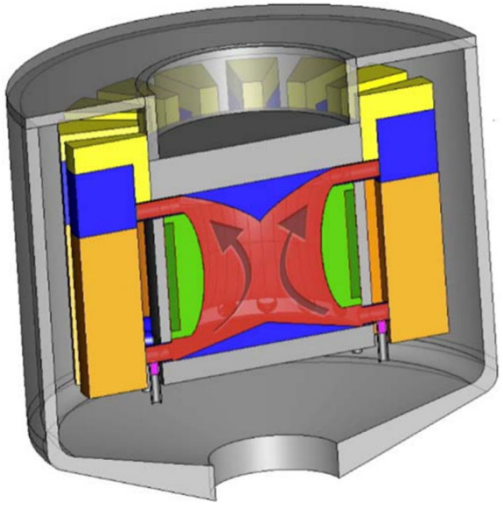

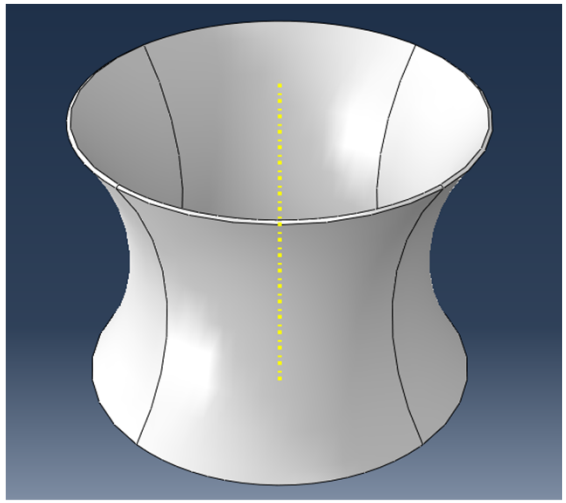

SAM SAFER

Model and boundary conditions

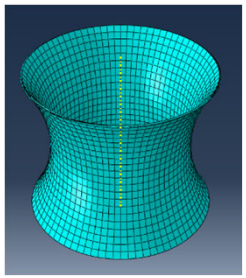

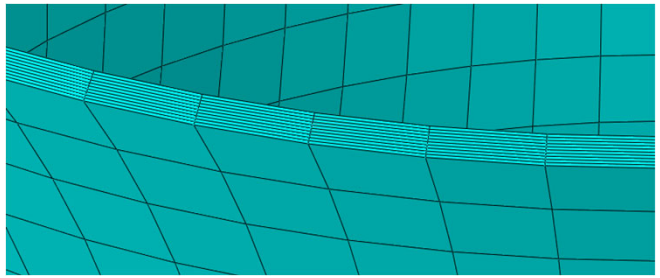

- Geometry according to current design
- 2D axialsymmetric analysis
- Mesh with C3D8T elements
- Object is cantilevered at the bottom and free at the top

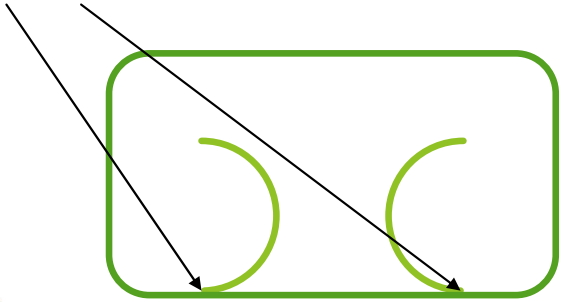

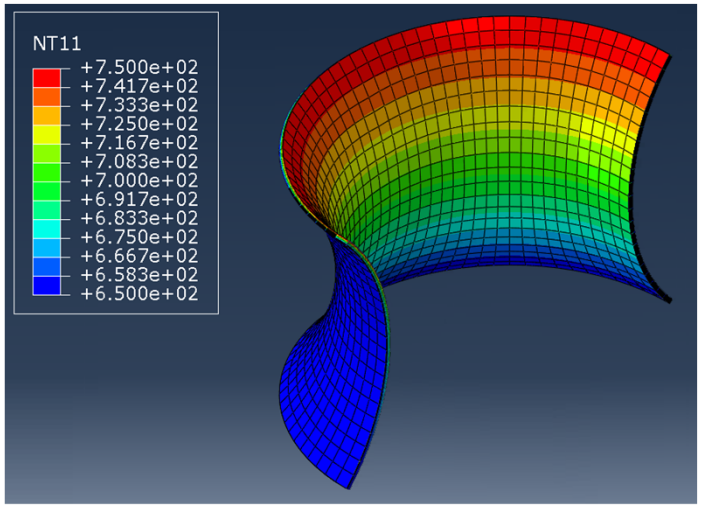

- Design temperature profile derived from Task 4.1
- Outer temperature assumed to be uniform
- Control of outer temperature is key to minimize thermal stresses

SAM SAFER

Stresses and displacements

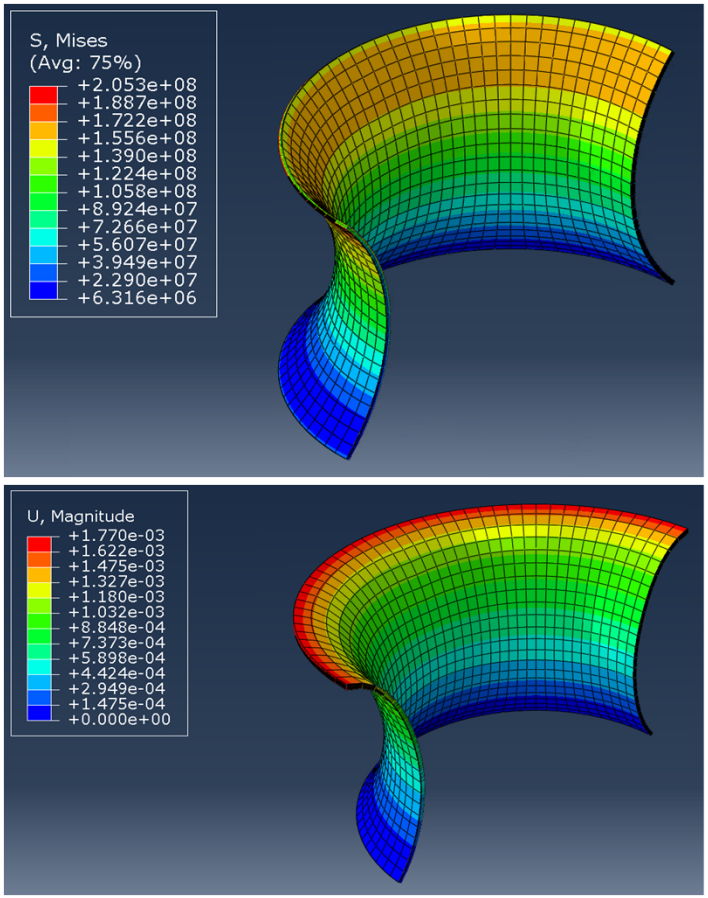

- Thermal stresses in the confinement are below the yield strength of the material
- The displacements are compatible with the connection of the confinement to other components
- The proposed cantilever at the bottom implies higher displacement and stresses at the top of the confinement
- Detailed design of the top part of the confinement and of its connections to other components is recommended
- Hastelloy N, with a thickness of 3 cm, and a uniform outer temperature of 650°C is considered as a reliable preliminary design

SAM SAFER

Creep verification

- Temperatures in the confinement are well above $T/T_m = 0.4$
- Thermal creep verification is thus performed

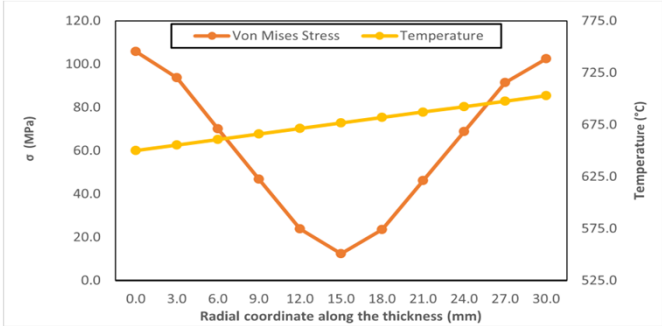

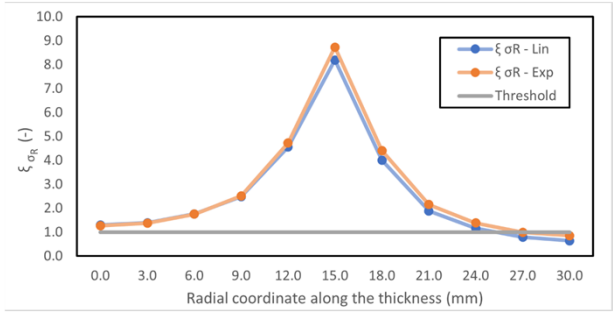

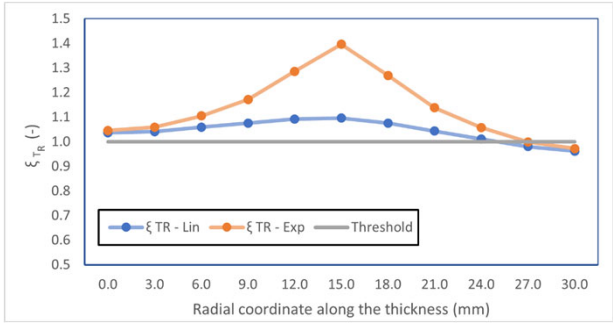

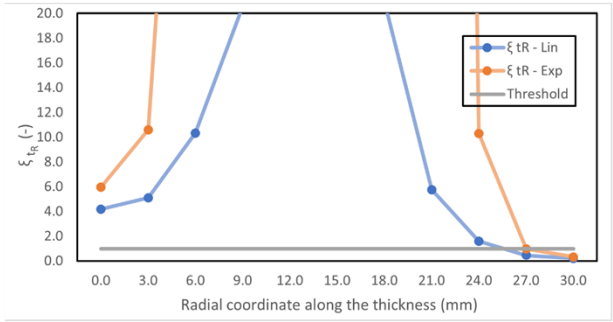

- Far from discontinuities, the bulk of the confinement is able to withstand thermal creep
- Margin with respect to temperature variations is limited, calling for as limited fluctuations as possible in normal operating conditions
- Margin towards thermal stresses can be increased by insulating the component on the outer surface (i.e., reducing the thermal gradient across its thickness)

SAM SAFER

Thank you for your kind attention!

SAM SAFER